

**EXPERIMENTAL AND NUMERICAL STUDY OF LAMINAR FORCED
CONVECTION HEAT TRANSFER FOR A DIMPLED HEAT SINK**

A Thesis

by

DO SEO PARK

Submitted to the Office of Graduate Studies of
Texas A&M University
in partial fulfillment of the requirements for the degree of
MASTER OF SCIENCE

August 2007

Major Subject: Mechanical Engineering

**EXPERIMENTAL AND NUMERICAL STUDY OF LAMINAR FORCED
CONVECTION HEAT TRANSFER FOR A DIMPLED HEAT SINK**

A Thesis

by

DO SEO PARK

Submitted to the Office of Graduate Studies of
Texas A&M University
in partial fulfillment of the requirements for the degree of

MASTER OF SCIENCE

Approved by:

Chair of Committee,	Egidio E. Marotta
Committee Member,	S.C. Lau
	Tahir Cagin
Head of Department,	Dennis L. O'Neal

August 2007

Major Subject: Mechanical Engineering

ABSTRACT

Experimental and Numerical Study of Laminar Forced Convection Heat Transfer
for a Dimpled Heat Sink. (August 2007)

Do Seo Park, B.En., Korea University

Chair of Advisory Committee: Dr. Egidio (Ed) Marotta

An investigation was conducted to determine whether dimples on a heat sink fin can increase heat transfer for laminar airflows. This was accomplished by performing an experimental and numerical investigation using two different types of dimples: 1) circular (spherical) dimples, and 2) oval (elliptical) dimples. Dimples were placed on both sides of a copper plate with a relative pitch of $S/D=1.21$ and relative depth of $\delta/D=0.2$ (e.g., circular dimples). For oval dimples, similar ratios with the same total depth and circular-edge-to-edge distance as the circular dimples were used. For those configurations the average heat transfer coefficient and Nusselt number ratio were determined experimentally. For circular and oval dimples, heat transfer enhancements (relative to a flat plate) were observed for Reynolds number range from 500 to 1650 (Reynolds number based on channel height). Moreover, pressure drop, thermal performance and flow characteristic were simulated numerically.

This experiment and numerical investigation was undertaken to provide the needed experimental data and numerical simulations that fill the gap for the use of dimples for laminar flow conditions. Specifically, this investigation was conducted to

determine whether or not the use of dimples can enhance heat transfer characteristics for heat sink applications. The heat transfer coefficients of the numerical results were very close to the experiment results. Dimples enhanced heat transfer from its surface for laminar air flows while the pressure drop was equivalent or smaller than that of the flat surface. These surfaces do indeed enhance thermal performance without the penalty associated with higher pressure drops.

ACKNOWLEDGMENTS

I would like to thank my committee chair, Dr. E. E. Marotta, and my committee members, Dr. S. C. Lau and Dr. Tahir Cagin, for their guidance and support throughout the course of this research.

My sincere appreciation also goes to my friends and colleagues who have spent many hours in discussion with me.

Finally, I am thankful to my family, and fiancé for their encouragement, patient support, and love.

TABLE OF CONTENTS

	Page
ABSTRACT	iii
ACKNOWLEDGMENTS.....	v
TABLE OF CONTENTS	vi
LIST OF FIGURES.....	viii
LIST OF TABLES	x
NOMENCLATURE.....	xi
 CHAPTER	
I INTRODUCTION.....	1
1.1 Objectives.....	1
1.2 Outline.....	4
II LITERATURE REVIEW.....	5
2.1 Experimental Studies.....	5
2.2 Numerical Studies	8
III EXPERIMENTAL DETAIL.....	10
3.1 Introduction	10
3.2 Experimental Setup	10
3.3 Experimental Procedure	16
3.4 Data Reduction.....	18
3.5 Uncertainty.....	19
IV NUMERICAL DETAIL.....	21
4.1 Introduction	21
4.2 Mathematical Model	21
4.3 Computation Procedure.....	22
4.3.1 Computational Grid.....	22

CHAPTER	Page
4.3.2 Computational Model	24
4.3.3 Grid Independence and Solution Convergence	24
V RESULTS AND DISCUSSION	28
5.1 Introduction	28
5.2 Experimental Results for Heat Transfer Enhancement	28
5.3 Numerical Predictions	31
5.3.1 Average Heat Transfer Coefficient	31
5.3.2 Pressure Drop	33
5.3.3 Thermal Performance	33
5.3.4 Flow Structure	36
5.4 Summary of Experimental Results and Numerical Predictions	41
VI CONCLUSIONS AND RECOMMENDATIONS.....	49
REFERENCES	52
APPENDIX A	56
VITA	60

LIST OF FIGURES

FIGURE	Page
3.1 Schematic drawing of the test equipment	11
3.2 Test section	12
3.3 CPU and heat sink with circular dimples.....	14
3.4 Test section of: (a) a general square channel, (b) present experimental channel	14
3.5 Schematic drawings, (a) the entire test surface of the flat copper plate; (b) the entire test surface of the circular type copper plate with dimple dimensions ; (c) the entire test surface of the oval (elliptical) type copper plate with dimple dimensions.....	15
3.6 Thermocouple location	17
4.1 Geometry detail for numerical model	23
4.2 The side and top views of the circular dimple plate	25
4.3 The side and top views of the oval dimple plate.....	26
5.1 Heat transfer coefficient for the copper plates	29
5.2 Heat transfer enhancement on the dimple plates.....	30
5.3 Heat transfer enhancement on the dimple plates.....	32
5.4 Friction factor ratio, f/f_0	34
5.5 Thermal performance for circular and oval dimpled plate.....	35
5.6 Schematic diagram of planes used to compute the streamwise development over dimples	37
5.7 Streamline of upstream and downstream for the flat plate.....	38
5.8 Streamline of upstream and downstream for the circular dimpled plate.....	39

FIGURE	Page
5.9 Streamline of upstream and downstream for the oval dimpled plate	40
5.10 Downstream spanwise sectional view for the circular dimpled plate	43
5.11 Downstream spanwise sectional view for the oval dimpled plate	44
5.12 Streamwise top view over the flat plate	45
5.13 Streamwise top view over the circular dimpled plate	46
5.14 Streamwise top view over the oval dimpled plate.....	47
5.15 Streamwise top view inside of the dimples	48

LIST OF TABLES

TABLE	Page
4.1 The number of finite volume cells for each domain	24
4.2 The three different sets of grids for grid independent check.....	27
A.1 Maximum uncertainties of measured data for air mass flow rate	58
A.2 Maximum uncertainties of measured data for heat transfer coefficient.....	59
A.3 Maximum uncertainties of all calculated data.....	59

NOMENCLATURE

A_S	=	surface area [m ²]
H	=	channel height [m]
D	=	dimple print diameter [m]
I	=	current supplied the heater [A]
T_w	=	average wall temperature [K]
T_b	=	mean bulk temperature [K]
$T_{b,inlet}$	=	inlet bulk temperature [K]
$T_{b,outlet}$	=	outlet bulk temperature [K]
C_p	=	specific heat [K]
Nu	=	overall average Nusselt number
Nu_0	=	overall average Nusselt number of a flat plate
f	=	friction factor
f_0	=	friction factor of a flat plate
K	=	thermal conductivity [Wm ⁻¹ K ⁻¹]
m	=	mass flow rate of air [kgs ⁻¹]
S	=	dimple pitch [m]
h	=	average heat transfer coefficient [Wm ⁻² k ⁻¹]
Q_{total}	=	heat transfer from heater [W]
Q_{loss}	=	extraneous heat loss [W]
Q_{net}	=	net heat transfer rate [W]

V = voltage across the heater [V]

Greek Symbols

ρ = density of air [kgm^{-2}]

δ = dimple depth [m]

CHAPTER I

INTRODUCTION

1.1 Objectives

The importance of heat transfer enhancement has gained greater significance in such areas as microelectronic cooling, especially in central processing units, macro and micro scale heat exchangers, gas turbine internal airfoil cooling, fuel elements of nuclear power plants, and bio medical devices. A tremendous amount of effort has been devoted to developing new methods to increase heat transfer from finned surface to the surrounding flowing fluid. Rib turbulator, an array of pin fins, and dimples have been employed for this purpose.

In case of the electronics industry, due to the demand for smaller and more powerful products, power densities of electronic components have increased. The maximum temperature of the component is one of the main factors that control the reliability of electronic products. Thermal management has always been one of the main issues in the electronics industry, and its importance will grow in coming decades.

The use of heat sinks is the most common application for thermal management in electronic packaging. Heat sink performance can be evaluated by several factors: material, surface area, flatness of contact surfaces, configuration, and fan requirements.

This thesis follows the style of International Journal of Heat and Mass Transfer.

Aluminum is the most common material because of its high conductivity (205W/mK), low cost, low weight, and easiness with respect to manufacturability. Copper is also used for heat sinks because of very high conductivity (400W/mK), but its disadvantages include high weight, high price, and less choices as far as production methods. To combine the advantages of aluminum and copper, heat sinks can be made of aluminum and copper bonded together. To improve performance, heat sinks should be designed to have a large surface area since heat transfer takes place at the surface. In addition, flatness of the contact surface is very important because a nominally flat contact area reduces the thermal interface resistance between the heat sink and heat source. A heat sink must be designed to allow the cooling fluid to reach all cooling fins and to allow good heat transfer from the heat source to the fins. Heat sink performance also depends on the type of fluid moving device used because airflow rates have a direct influence on its enhancement characteristics.

To obtain higher performance from a heat sink, more space, less weight, and lower cost are necessary. Thus, efforts to obtain more optimized designs for heat sinks are needed to achieve high thermal performance.

One method to increase the convective heat transfer is to manage the growth of the thermal boundary layer. The thermal boundary layer can be made thinner or partially broken by flow disturbance. As it is reduced, by using interrupted and/or patterned extended surfaces, convective heat transfer can be increased. Pin fins, protruding ribs (turbulators), louvered fins, offset-strip fins, slit fins and vortex generators are typical methods. The pattern and placements are suitably chosen based on the required cooling.

Heat transfer augmentation using these methods always results in pressure drop penalties that adversely affect the aerodynamics and efficiencies. In the case of cooling of turbine blades, surface protrusions induce excessive pressure losses, which increase the compressor load. The separated flow field over ribs or pin fins can make significant non-uniform cooling, which leads to thermal stresses.

For the case of concavities or dimples on the surfaces of internal flow passages, it produces substantial heat transfer augmentations, with pressure drop penalties that are smaller than other types of heat transfer augmentations. This is accomplished by not protruding into the flow region and thus, not increasing the friction loss due to skin friction. Because of easiness in manufacturing, dimples are also attractive as a heat transfer augmentation device.

Although there are a few investigations for the use of dimples under laminar airflow conditions, there exist no experimental data with respect to the use of different dimple shapes for heat sink applications. Therefore, this study evaluated the heat transfer characteristics using two different dimple shapes on a heat sink fin by experimental and numerical methods: 1) circular (spherical) dimples, and 2) oval (elliptical) dimples. The average heat transfer coefficient and heat transfer performance were obtained experimentally. Heat transfer coefficient, pressure drop, thermal performance and flow characteristics were simulated numerically.

1.2 Outline

Chapter II, which follows, shows a literature review of the experimental and numerical work on heat transfer enhancement using dimples. Chapter III gives an account of the experimental set up for this research, including test equipment and sample preparation. Chapter IV gives numerical details for this study. The results and uncertainty of the experimental runs and numerical simulation are described in Chapter V. A summary and conclusions from this research are presented in Chapter VI.

CHAPTER II

LITERATURE REVIEW

Due to dimples heat transfer enhancement characteristics and lesser pressure loss penalties, their use for thermal management application has attracted many researchers. One of the earliest research studies on dimples was conducted by Bearman and Harvey [1], who experimentally showed that dimpled circular cylinders can reduce drag force by affecting flow conditions around the circular cylinder similar to dimples on a golf ball. Until now, numerous experimental and numerical studies exist for the use of dimples for turbulent flow, but very little data exist for laminar flow regimes.

2.1 Experimental Studies

Several parameters were chosen to evaluate the effects of dimples: Reynolds number (Re_H), relative channel height (H/D), relative dimple depth (δ/D), and turbulent intensity. Many investigations have been conducted for a rectangular channel. Chyu et al. [2] studied the enhancement of surface heat transfer in a channel using two different concavities- hemispheric and tear drop. Concavities serve as vortex generators to promote turbulent mixing in the bulk flow to enhance the heat transfer at $Re_H = 10,000$ to $50,000$, H/d of 0.5 , 1.5 , 3.0 and $\delta/d = 0.575$. Heat transfer enhancement was 2.5 times higher than smooth channel values and with very low pressure losses that were almost

half that caused by conventional ribs turbulators. Moon et al. [3] experimentally studied the effect of channel height on heat transfer performance and friction losses in a rectangular dimpled passage with staggered dimples on one wall. The geometry used was $H/D = 0.37, 0.74, 1.11, 1.49$ and $Re_H = 12,000$ to $60,000$. Heat transfer enhancement was roughly 2.1 times greater than the smooth channel configuration with H/D values from 0.37 to 1.49. The heat transfer augmentation was invariant with the Reynolds number and channel height. The increase in friction factor was 1.6 to 2.0 times less than the smooth channel. The pressure losses also remained approximately constant for the channel height. Mahmood et al [4] studied the flow and heat transfer characteristics over staggered arrays of dimples with $\delta/D=0.2$. For the globally average Nusselt number, there were small changes with Reynolds number. Ligrani et al [5] studied the effect of dimpled protrusions (bumps) on the opposite wall of the dimpled surface.

Mahmood et al [6] experimentally showed the influence of dimple aspect ratio, temperature ratio, Reynolds number and flow structures in a dimpled channel at $Re_H = 600$ to $11,000$ and air inlet stagnation temperature ratio of 0.78 to 0.94 with $H/D = 0.20, 0.25, 0.5, 1.00$. The results indicated that the vortex pairs which are periodically shed from the dimples become stronger and local Nusselt number increase as channel height decreases. As the temperature ratio T_{oi}/T_w decreases, the local Nusselt number also increased.

Burgess et al [7] experimentally analyzed the effect of dimple depth on the surface within a channel with the ratio of dimple depth to dimple printed diameter, equal

to δ/D , 0.1, 0.2, and 0.3. The data showed that the local Nusselt number increased as the dimple depth increased due to an increased strength and intensity of vortices and three dimensional (3D) turbulent production. Ligrani et al [8] studied the effect of inlet turbulence level in the heat transfer improvement in walls with dimple ratio $\delta/D=0.1$, showing that as the turbulence level was increased, the relative Nusselt number reduced due to the increased turbulent diffusion of vorticity.

Bunker et al [9] use circular pipes with in-line arrays of dimples with $\delta/D=0.2$ and 0.4 and surface area densities ranging from 0.3 to 0.7 to provide heat transfer enhancement and friction effects of dimples in a circular tube. Reynolds numbers for bulk flow were from 20,000 to 90,000. Heat transfer enhancement was 2times greater than the smooth circular tube in the case where the relative dimple depth was greater than 0.3 and array density was greater than 0.5. An increase of friction factor was approximately 4 to 6 times greater than the smooth circular tube, which was better than the rib turbulartors. Han [10] studied the rotational effect of dimples in turbine blade cooling. In the case where a pressure drop is the main design concern, dimple cooling can be a good choice. Jet impingement over a convex dimpled surface was studied by Chang et al. [11] showing an incremental increase in the relative Nusselt number (Nu/Nu_0) up to 1.5.

An investigation for the use of dimples for heat sink fin applications was conducted by Small et al. [12], who experimentally and numerically studied heat sinks, for a mock microprocessor, with dimpled surfaces. A heat sink with a staggered array of

9, 8 and 9 rectangular fins with dimpled surfaces showed the best performance with less volume (about 25% less than the set value) usage.

2.2 Numerical Studies

Many numerical studies also have been performed for dimpled surfaces. Lin et al. [13] present computational simulation results for a channel in which the walls were lined with four rows of hemispherical cavities in a turbulent airflow condition. Isaev et al. [14-19], studied the effect of dimples emphasis on the flow structure and heat transfer characteristics in a laminar and a turbulent airflow condition. A relative dimple depth in the range of 0.06 to 0.24 and a SIMPLEC (Semi-Implicit Method for Pressure-Linked Equations) method with multiblock grids were used to evaluate the flow change and heat transfer enhancement characteristics. They also studied the effect of Reynolds number (both laminar and turbulent) over dimples of $\delta/D = 0.22$. These numerical studies focused on the flow structure and heat transfer, with only brief mention of pressure drops and drag coefficients. The geometry and flow conditions were the same to that used by Chyu et al [2] to compare with the computed results. This study explained the flow structure and heat transfer enhancement characteristics induced by concavities.

Park et al. [20] numerically examined turbulent airflow in a channel with deep dimples ($\delta/D = 0.3$) using the Realizable $k-\epsilon$ model and no wall function for $Re_H = 2,700$ to 41,000. This study provided details of the development of flow structures through the dimples and their subsequent impact on heat transfer. However, the

numerical data (heat transfer enhancement pattern and value) were not in good agreement with experiment data. Park et al. [21] also studied seven different geometries (1-spherical, 2-cylindrical and 4-triangular) presenting relative Nusselt numbers, velocity and Eddy diffusivity distributions. Spherical and tilted cylindrical dimples showed the best thermal performance.

A numerical study based on the Response-Surface Method (RSM) was performed by Kim [22] to optimize the shape of a dimple for better turbulent heat transfer and friction losses. The numerical data were compared with the experimental results from Bunker et al [6]. Kim [22] calculated the optimum relative depth and relative pitch to be 0.24 and 1.81 respectively. Silva et al [23] showed flow structure and optimum value of the relative pitch from 0.81 to 1.21.

Therefore, this experiment and numerical investigation was undertaken to provide the needed experimental data and numerical simulations that fill the gap for the use of dimples for laminar flow conditions. Specifically, this investigation was conducted to determine whether or not the use of dimples can enhance heat transfer characteristics for heat sink applications.

CHAPTER III

EXPERIMENTAL DETAIL

3.1 Introduction

In this chapter, a description of the experimental setup is presented with a discussion of the experimental procedure, data reduction, and uncertainty of the experiment in this section.

3.2 Experimental Setup

A schematic drawing of the facility used for heat transfer measurements is shown in Fig. 3.1. The average heat transfer coefficient on the plate surface was measured for various rates of airflow through the channel. It consists of an open loop flow circuit. The main components of the test apparatus are a test section, a rectangular channel, a plenum, a calibrated orifice flow meter, a gate valve, and a centrifugal blower. The channel inner cross section dimensions are 32mm (wide) and 103.5mm (height). The entrance channel is 2500mm long. The channel was constructed with 8.3mm thick acrylic plates with thermal conductivity $k=0.16\text{W/mk}$ at $20\text{ }^\circ\text{C}$ to minimize heat losses. A 300x300x450mm plenum with wood was fabricated to stabilize the flow drawn by the blower. Figure 3.2 shows the cross section of the test section. All exterior surfaces of the test section are insulated with fiberglass ($k=0.04\text{W/mk}$) to minimize heat losses. Omega electric heaters model KH-108/5-P (Kapton heater, 25.4x203.2mm, 115 Volts, 40 W

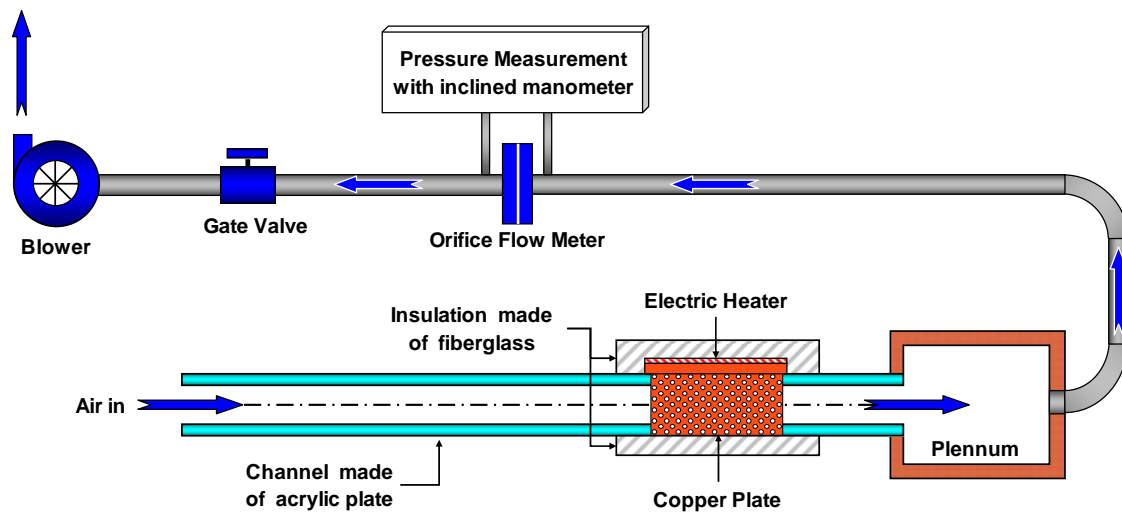


Fig. 3.1 Schematic drawing of the test equipment

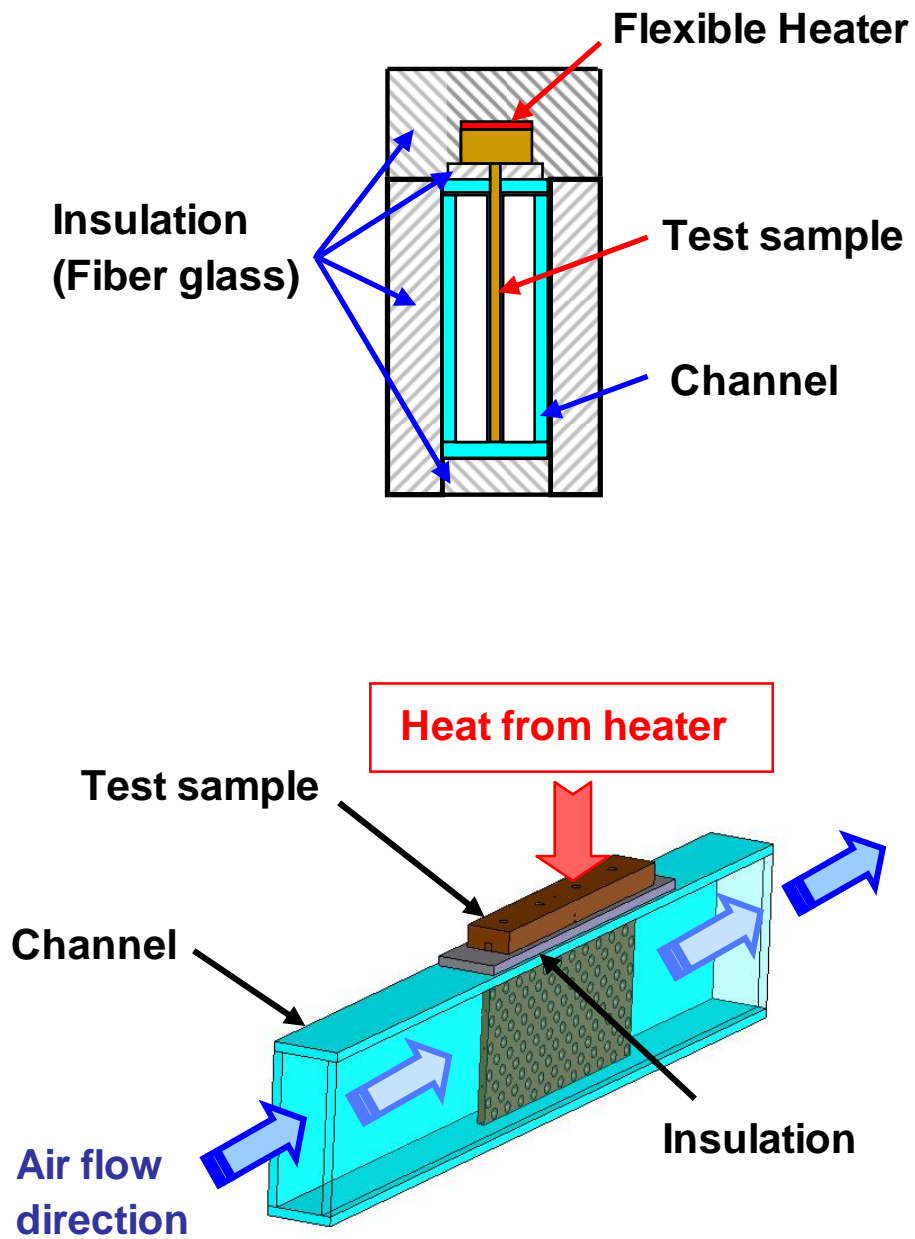


Fig. 3.2 Test section

total power, pressure sensitive adhesive on one side) is used to provide a constant heat flux to the copper plate. The heaters allowed a heat flux up to 40 kW/m^2 through the 5mm-thick test plate.

Power was supplied by an Elenco Precision variable power supply model XP-800, with multi-meters TENMA 72-6685A and 72-6185 used to measure voltage and current into the heater.

Fig 3.3 shows the CPU and heat sink with dimples. Only one fin was used to study and quantify the heat transfer enhancement characteristics. For the case of internal heat convection test with a square channel, a uniform heat flux is applied from the bottom of the plate in Fig 3.4(a). For this study, heat flux was applied from top of the plate to simulate similar test conditions for an actual heat sink application, as shown in Fig 3.4(b).

Figs 3.5 (a), (b), and (c) present the geometric details of the test surface including dimple geometry. Fig 3.5(b) shows the circular dimpled plate with 11 by 22 dimples and Fig 3.5(c) shows the oval (elliptical) dimpled plate with 7 by 22 dimples on each side. The dimples were placed on both sides of the copper plate with a relative pitch $S/D=1.21$ and a relative depth $\delta/D=0.2$ for the circular dimples. For the oval dimples, $S/D=1.21$ and $\delta/D=0.2$ with same total depth and circular-edge-to-edge distance as the circular dimples. Three test plates were fabricated with 5mm thickness ASTM B152 Electroless Oxygen-Free Copper. Because a flat projected area was used to calculate a heat transfer coefficient and a Nusselt number, the total surface area for each plate was constant.

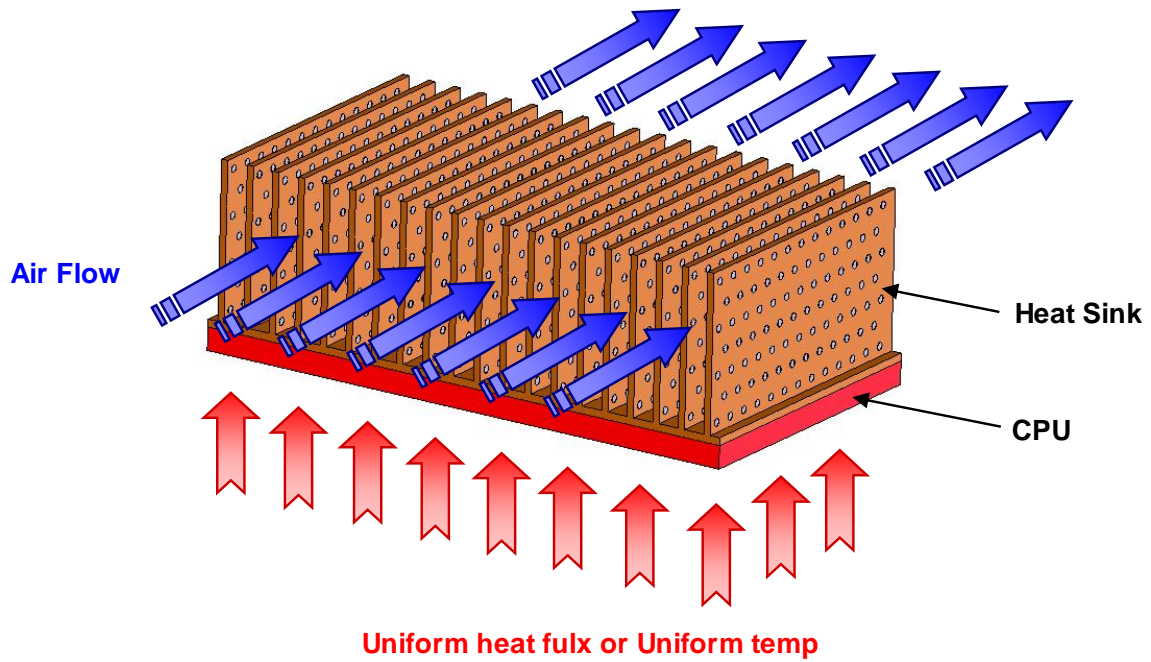


Fig. 3.3 CPU and heat sink with circular dimples

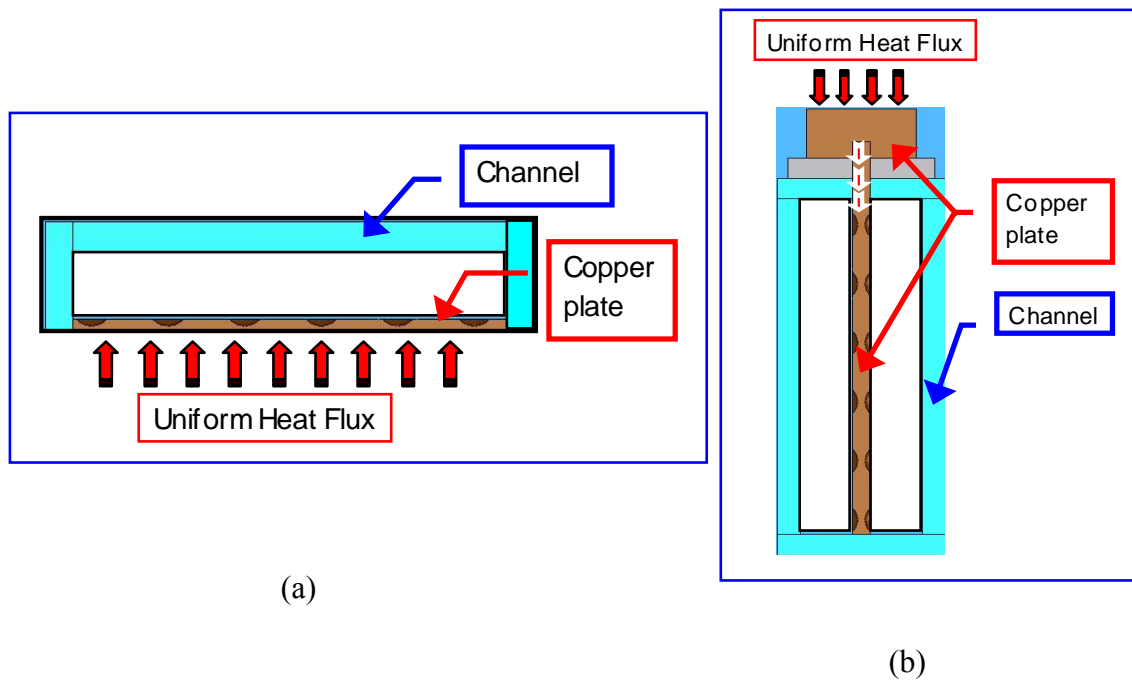
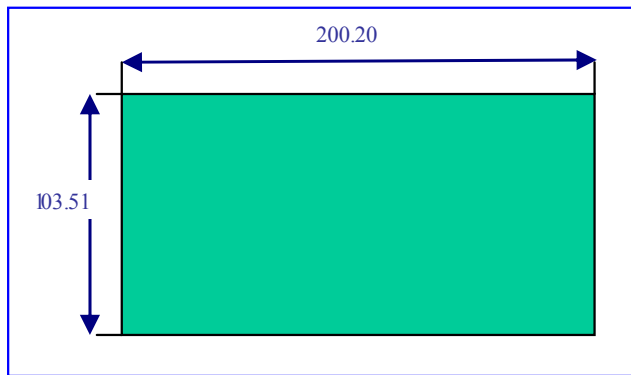
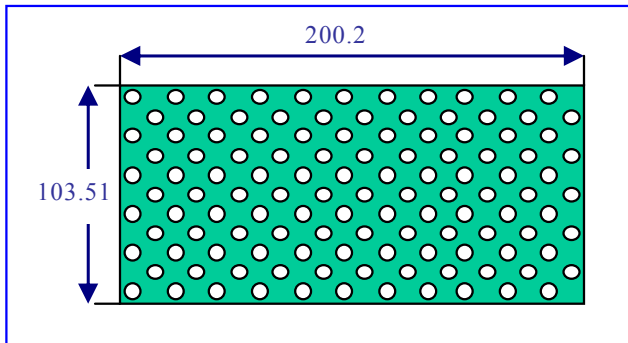


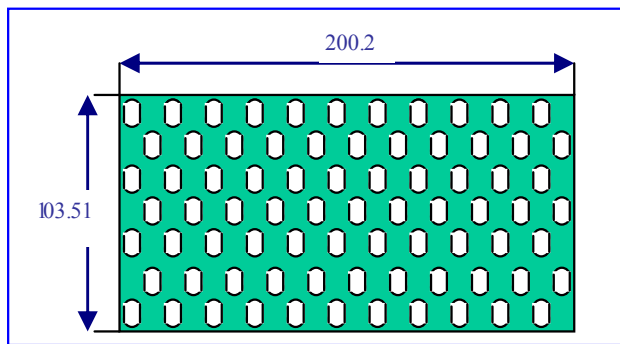
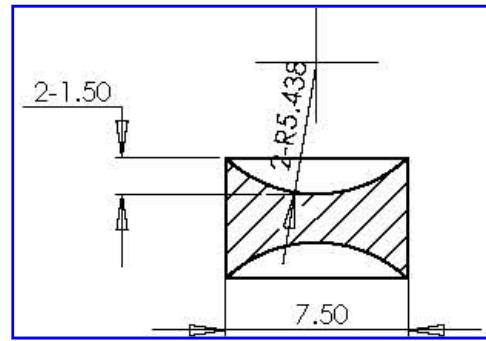
Fig. 3.4 Test section of: (a) a general square channel, (b) present experimental channel



(a)



(b)



(c)

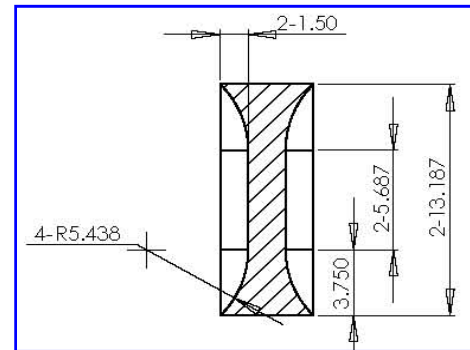


Fig. 3.5 Schematic drawings, (a) the entire test surface of the flat copper plate; (b) the entire test surface of the circular type copper plate with dimple dimensions ; (c) the entire test surface of the oval (elliptical) type copper plate with dimple dimensions. All dimensions are given in mm

The temperature of the copper plate was measured using nine (9) calibrated copper-constantan thermocouples. Fig 3.6 shows the thermocouples locations. Six (6) thermocouples were located inside the copper plate to obtain the average temperature of the plate and four (4) thermocouples were used to measure the heat flux from the flexible heater. Additional thermocouples were used at the channel inlet and outlet and at the ASME orifice plate in order to obtain air inlet temperature and temperature corrections for the volumetric airflow. Thermocouples were connected to a National Instruments data acquisition unit model SCXI-1000, and then to a PC running Lab view 7.1. An inclined manometer measured the pressure drop across the orifice, and a pressure transducer measured the pressure upstream of the orifice. These pressures were used to calculate the mass flow rate of air through the test section during an experiment.

3.3 Experimental Procedure

The copper plate was located in the middle of the test channel. Care was taken so that the copper plate can be located in the middle of the test section in order to ensure an equal channel height conditions and airflow rates for both sides of the copper plate. The outer surface of the test section consisted of fiberglass to reduce heat loss to the outside surroundings.

The blower was turned on and air was forced through the test setup. The flow rate through the test section was controlled with the help of a valve downstream of the orifice plate. The flow rate was set in such a way so that the pressure drop across the orifice corresponds to the required Reynolds number.

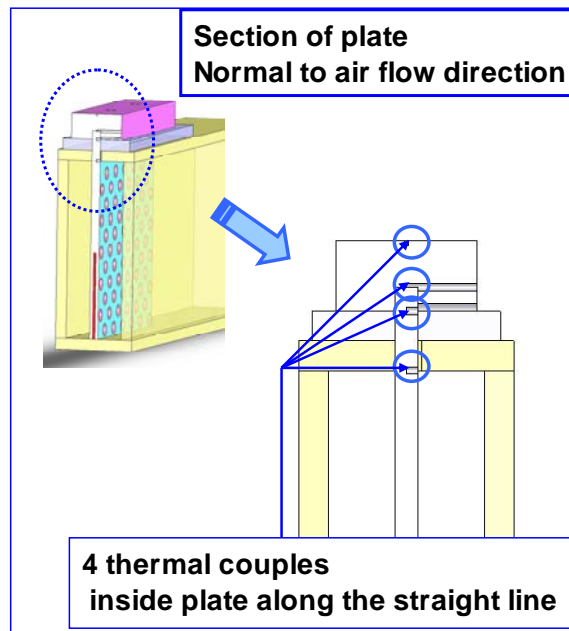
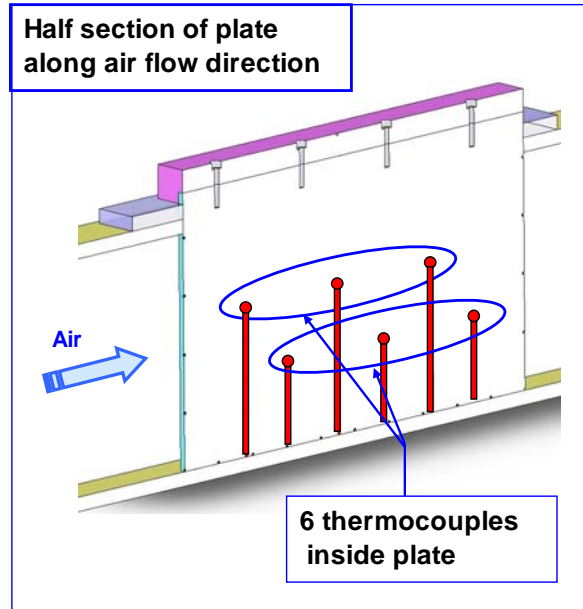


Fig. 3.6 Thermocouple location

After the flow was set across the test section, the heaters were turned on and the voltage supplied to the heaters was roughly set to 14W. According to the temperature of the copper plate, voltage and current were changed. After the measured temperatures reached a specific value, the voltage was controlled to an input power 14W.

After an elapsed time of roughly 14 hours, the temperature of the copper plate reached steady state. The pressure difference across the orifice was checked frequently so that the flow rate did not change from the intended value of Reynolds number. At steady state, the temperatures of the copper plate were checked by the data acquisition system and logged by the computer. The pressure difference across the orifice plate and the pressure across upstream of the orifice plate were measured. The voltage supplied to the heater and the corresponding current was taken to calculate the heat supplied to the copper plate. The temperatures of the inlet air into the test section and into the orifice plate were also checked.

3.4 Data Reduction

The objective of this investigation was to study the heat transfer characteristics using dimples at low Reynolds number flow conditions. An average heat transfer coefficient was calculated from the net heat transfer per unit area, the average temperature of the plate, and the bulk mean air temperature. To quantify the average heat transfer coefficient, the following expression was used:

$$h = \frac{Q_{net}}{A_s(T_w - T_b)} = \frac{Q_{total} - Q_{loss}}{A_s(T_w - T_b)} \quad (3.1)$$

where the net heat flux (Q_{net}) is the electrical power supplied to the heater(Q_{total}) minus the heat loss from the test section(Q_{loss}). A_s is the surface area of the plate where the heat convection occurs. T_w is a steady-state wall temperature and T_b is a mean bulk temperature.

$$Q_{total} = V \cdot I \quad (3.2)$$

Q_{total} was calculated from V , input voltage and I , the input current to the flexible heater. Q_{loss} was calculated by running the test without air flow under the same wall temperature obtained as the actual test with air flow. The amount of power input was the heat loss Q_{loss} . For the general case, heat loss was calculated to be roughly 5~10%. For this experiment, the heat loss was about 25%. The main reason was insulation problems.

A mean bulk temperature, T_b , was determined by Eq. 3.3 where $T_{b, inlet}$ is the inlet bulk temperature and $T_{b, outlet}$ is the outlet bulk temperature that can be calculated from Eg. 3.4:

$$T_b = \frac{T_{b, inlet} + T_{b, exit}}{2} \quad (3.3)$$

$$T_{b, exit} = T_{b, inlet} + \frac{Q_{total} - Q_{loss}}{\dot{m}C_p} \quad (3.4)$$

3.5 Uncertainty

The uncertainty of the average heat transfer coefficient depends on the uncertainties in the average wall temperature, bulk air temperature difference, and the net heat input for each test section. This uncertainty increases with decreasing both the average wall temperature to bulk air temperature difference and the net heat flux. Based

on a confidence level of 95% described by Kline and McClintock [24], uncertainty value of $\pm 0.5\%$ for all properties of the air, and $\pm 0.5\%$ for all physical dimensions were used.

Based on the maximum uncertainties for pressure at the orifice flow meter, and the pressure drop across the orifice of $\pm 1.0\%$ and $\pm 4.1\%$, respectively, the maximum uncertainty of the air mass flow rate was calculated to be $\pm 2.8\%$. The corresponding maximum uncertainty of the Reynolds number was ± 2.9 . The uncertainty for the power input and heat loss were found to be $\pm 3.1\%$ and $\pm 5.4\%$, respectively, and those for the average wall and bulk temperatures $\pm 3.0\%$ and $\pm 3.5\%$, respectively. With these values, the uncertainty of the Nusselt number was calculated to be $\pm 7.8\%$.

CHAPTER IV

NUMERICAL DETAIL

4.1 Introduction

In this chapter, a description of the numerical simulation is presented with a discussion on the mathematical model, computational grid, and computational model for this section.

4.2 Mathematical Model

Fluid flow and heat transfer in a channel can be described mathematically by using three fundamental laws: The Principle of Mass Conservation, The Principle of Momentum Conservation and The Principle of Energy Conservation.

Fig 4.1 shows the geometric configuration under consideration. A uniform heat flux was applied to the top of the plate wall and heat convection occurs at the other surfaces of the plate except for the bottom surface of the plate where the condition is adiabatic. Assuming the thermophysical properties of the fluid and solid regions to be constant, the governing equations for the steady state can be written as:

Continuity Equation

$$\frac{\partial u}{\partial x} + \frac{\partial v}{\partial y} + \frac{\partial w}{\partial z} = 0 \quad (4.1)$$

Momentum Equations

$$\rho \left(u \frac{\partial u}{\partial x} + v \frac{\partial u}{\partial y} + w \frac{\partial u}{\partial z} \right) = -\frac{\partial P}{\partial x} + \frac{\partial}{\partial x} \left(\mu \frac{\partial u}{\partial x} \right) + \frac{\partial}{\partial y} \left(\mu \frac{\partial u}{\partial y} \right) + \frac{\partial}{\partial z} \left(\mu \frac{\partial u}{\partial z} \right) \quad (4.2)$$

$$\rho \left(u \frac{\partial v}{\partial x} + v \frac{\partial v}{\partial y} + w \frac{\partial v}{\partial z} \right) = -\frac{\partial P}{\partial y} + \frac{\partial}{\partial x} \left(\mu \frac{\partial v}{\partial x} \right) + \frac{\partial}{\partial y} \left(\mu \frac{\partial v}{\partial y} \right) + \frac{\partial}{\partial z} \left(\mu \frac{\partial v}{\partial z} \right)$$

$$\rho \left(u \frac{\partial w}{\partial x} + v \frac{\partial w}{\partial y} + w \frac{\partial w}{\partial z} \right) = -\frac{\partial P}{\partial z} + \frac{\partial}{\partial x} \left(\mu \frac{\partial w}{\partial x} \right) + \frac{\partial}{\partial y} \left(\mu \frac{\partial w}{\partial y} \right) + \frac{\partial}{\partial z} \left(\mu \frac{\partial w}{\partial z} \right)$$

Energy Equation

$$\rho C_p \left(u \frac{\partial T}{\partial x} + v \frac{\partial T}{\partial y} + w \frac{\partial T}{\partial z} \right) = \frac{\partial}{\partial x} \left(K \frac{\partial T}{\partial x} \right) + \frac{\partial}{\partial y} \left(K \frac{\partial T}{\partial y} \right) + \frac{\partial}{\partial z} \left(K \frac{\partial T}{\partial z} \right) \quad (4.3)$$

4.3 Computation Procedure

The computations of the fluid flow field and heat transfer were performed using CFD by Fluent software, version Fluent 6.2.16. Gambit 2.2.30 was used for the development of the computational grid.

4.3.1 Computational Grid

Numerical studies were conducted to determine the heat transfer and velocity profiles on the copper plate for laminar airflow in a rectangular channel. Fig 4.1 shows the tested geometry for the numerical model. The dimensions of the copper plates were the same as the experimental specimens. The entrance channel is 600mm long rectangular channel with a flow cross section of 33 mm (width) by 103.5mm (height). The exit channel is 1000mm long rectangular channel with a flow cross section of 33 mm (width) by 103.5mm (height). Because of symmetry in the flow direction, the numerical model was only solved for half of the channel and plate. This was helpful in reducing the need for more memory and the required processing time, which was

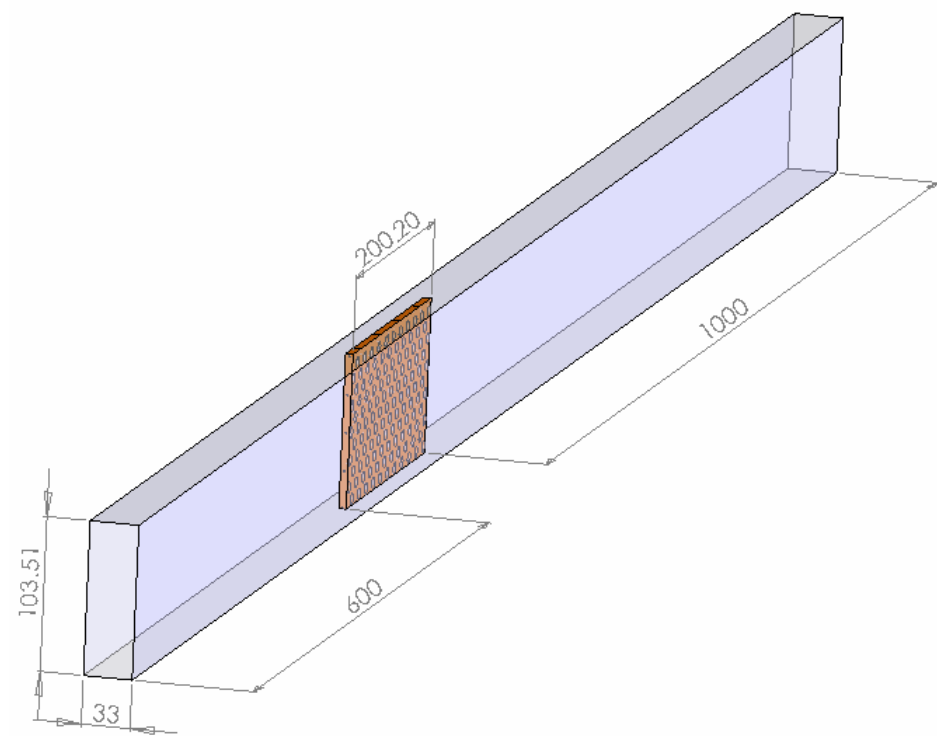


Fig. 4.1 Geometry detail for numerical model

especially critical for modeling the complex and detailed geometries of the dimpled heat sinks.

Fig 4.2 and 4.3 show side views and top views of the computational grid used for the circular dimples and oval dimples. Hexahedral elements aligned with the flow direction were used to reduce the numerical dissipation errors and improve the quality of numerical predictions. Fine grids were employed for near-wall and dimpled surfaces to resolve the high gradients encountered in these region. The numbers of finite volume hexahedral cells employed for the entire flow domain and each region are shown in Table. 4.1

Table 4.1 The number of finite volume cells for each domain

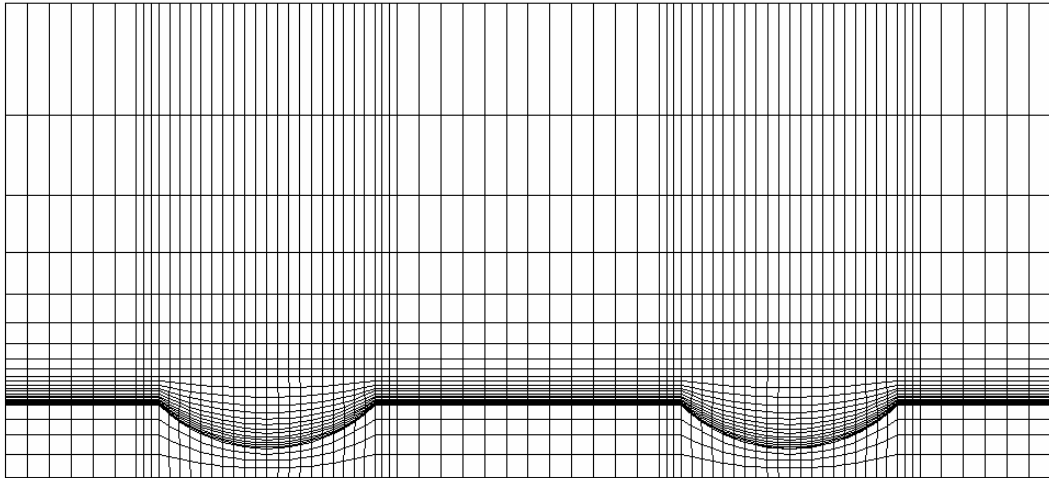
	Inlet Region	Plate Region	Outlet Region	Total
Flat	99,000	672,000	99,000	870,000
Circular	182,250	1,511,136	182,250	1,875,636
Oval	207,900	1,738,044	207,900	2,153,844

4.3.2 Computational Model

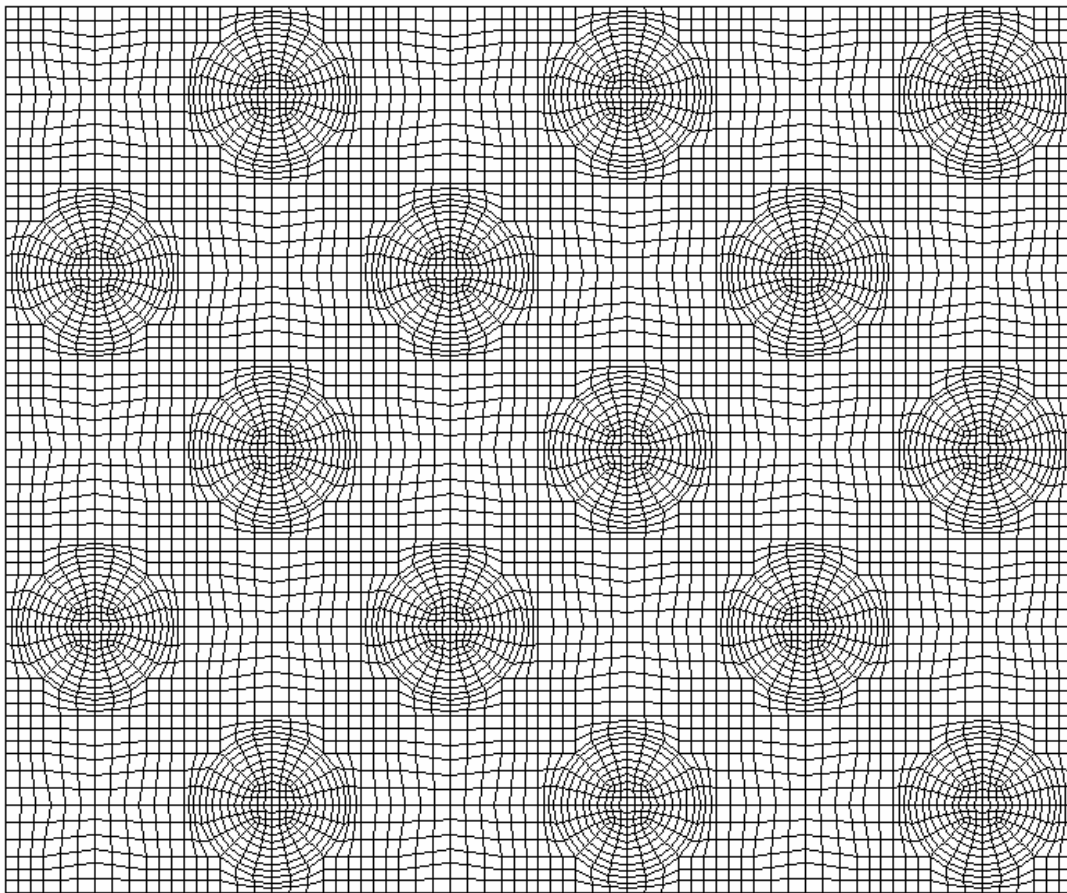
The SIMPLE (Semi-Implicit Method for Pressure-Linked Equations) algorithm, along with a structured grid, was used to couple the pressure and velocity fields. The second-order upwind interpolation scheme and second-order spatial discretization scheme were used to reduce numerical errors.

4.3.3 Grid Independence and Solution Convergence

Three different sets of grids were tested for grid independence of the circular dimpled plate: 6 by 8, 8 by 13, 10 by 16, 6 by 8 type were employed for circular and oval

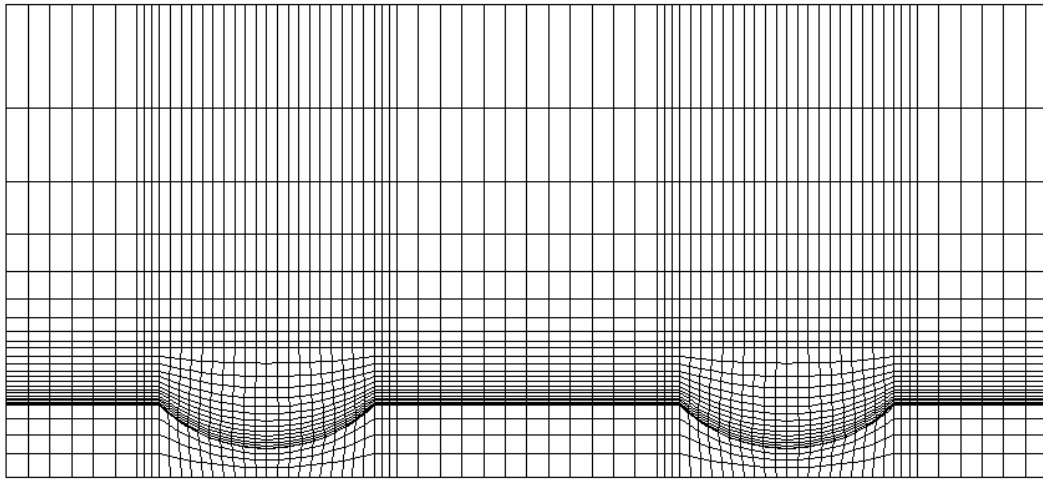


(a) the side view of the circular dimpled plate

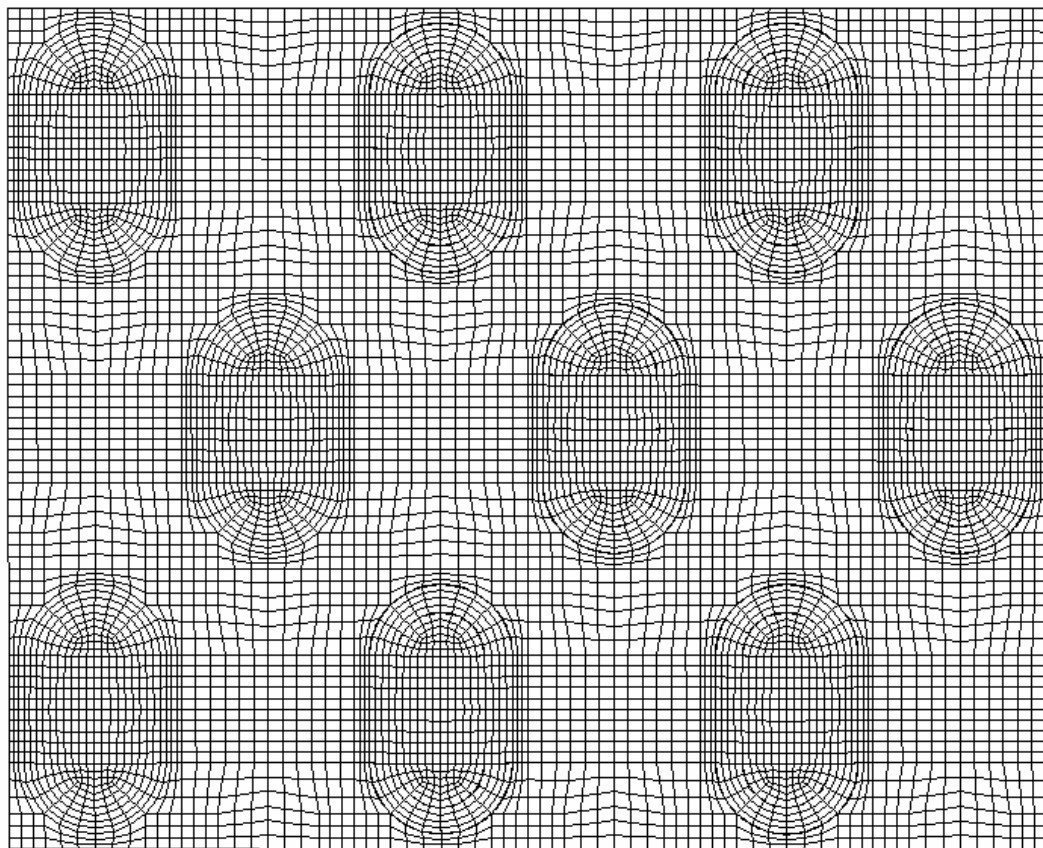


(b) the top view of the circular dimpled plate.

Fig. 4.2 The side and top views of the circular dimple plate



(a) the side view of the oval dimpled plate

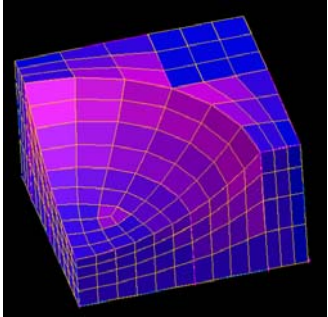
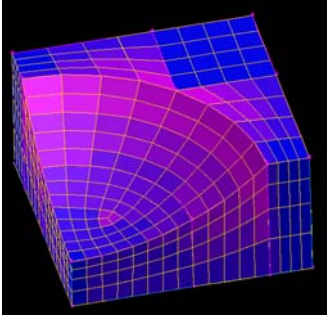
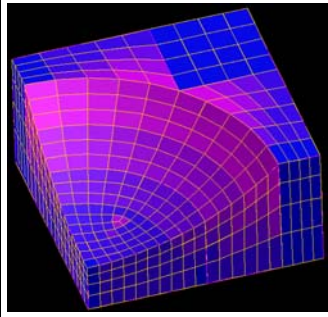


(b) the tope view of the oval dimpled plate

Fig. 4.3 The side and top views of the oval dimple plate

type dimple. Table 4.2 shows the three different sets of grids. It was found that heat transfer prediction varied less than 2 % with these grid selections.

Table 4.2 The three different sets of grids for grid independent check

	6 by 8 type	8 by 13 type	10 by 16 type
Shape			
Plate element number	1,219,488	1,995,296	2,607,776

The Implicit Method was employed to the computational iteration. Scaled residuals were used for the convergence of the computational solutions for the continuity, energy, and for the other predicted variables. The setting criterion of the scaled residuals for the solution convergence was 1×10^{-3} for all computed residuals except for the energy equation 1×10^{-6} .

CHAPTER V

RESULTS AND DISCUSSION

5.1 Introduction

This investigation presents both experimental and numerical studies for the heat transfer characteristics for a heat sink with laminar airflow conditions. This was conducted with two different types of dimples: 1) circular (spherical) dimples, and 2) oval (elliptical) dimples. The average heat transfer coefficient and Nusselt number ratio were obtained experimentally. Heat transfer, pressure drop, thermal performance and flow characteristics were numerically simulated.

5.2 Experimental Results for Heat Transfer Enhancement

Experiments using copper plates with a flexible heater were conducted to obtain Nusselt number ratio for a heat sink with dimpled surfaces in laminar airflow. Three different copper plates were fabricated and used to obtain the average heat transfer coefficient: flat, circular, and oval dimpled plates. Dimples were placed on both sides of the copper plate. Each plate was placed in the middle of the rectangular channel and a uniform heat flux was applied from the top of the plate. The flat plate was used as baseline data. Average heat transfer coefficients were calculated for four different Reynolds numbers based on channel height, Re_H from 500 to 1650 with a uniform heat flux of $1.4 \times 10^4 \text{ W/m}^2$.

Fig 5.1 shows the heat transfer coefficients for three different copper plates based

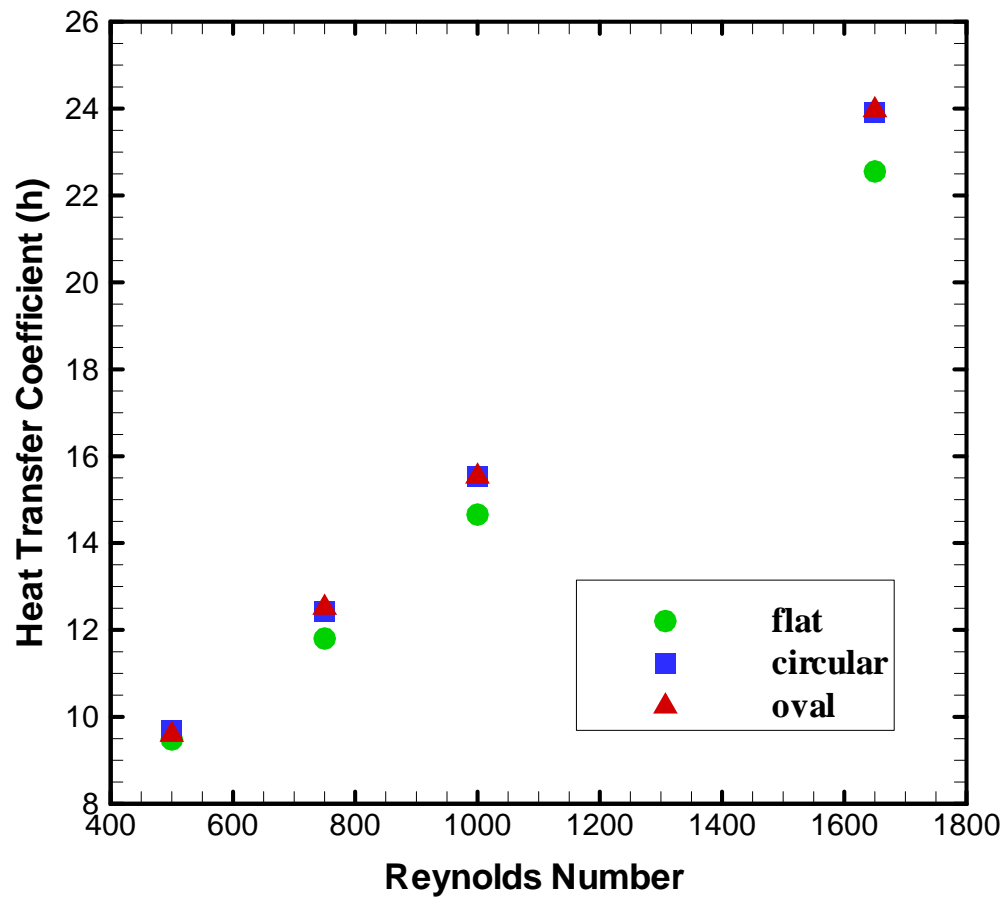


Fig. 5.1 Heat transfer coefficient for the copper plates

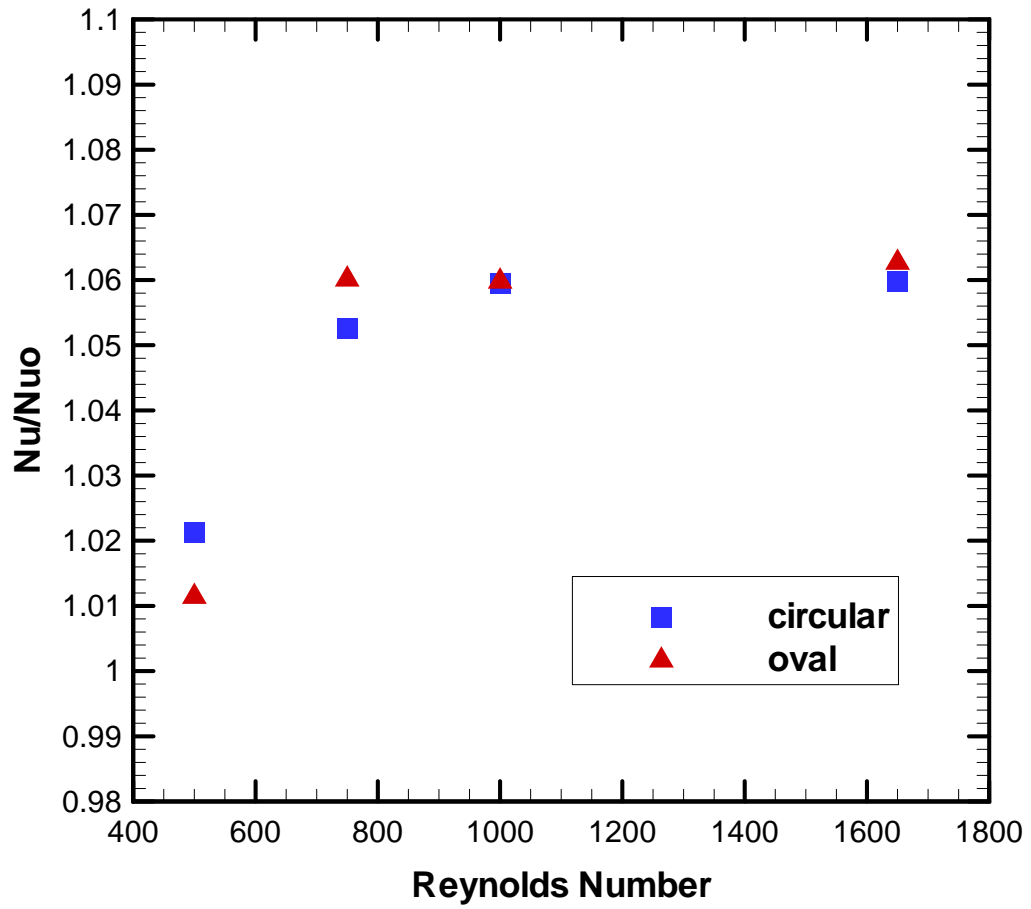


Fig. 5.2 Heat transfer enhancement on the dimple plates

on the flat projected area. The heat transfer coefficients increased with increasing airflow rate. The results showed that the heat transfer coefficients for the circular and oval dimpled plates were higher than that of the flat plate for all airflow conditions.

In Fig 5.2, the experimental results of the heat transfer enhancement characteristics for the circular and oval dimpled plates are presented. At very low flow velocity ($Re_H=500$), Nu/Nu_0 values for circular and oval type dimpled plate were less than 1.02. For Re_H from 750 to 1650, Nu/Nu_0 values for both circular and oval type cases are around 1.06 regardless of Re_H .

5.3 Numerical Predictions

The same geometries and test conditions as with the experimental specimens were used to simulated heat transfer coefficient, pressure drop, thermal performance, and flow characteristics using FLUENT version 6.2.16.

5.3.1 Average Heat Transfer Coefficient

All experimental test runs were selected for comparison with the numerical predictions. Geometrical features of the numerical model were the same as those of the experiments. Fig5.3 shows the heat transfer coefficients comparison of the experimental and numerical models for the four different Reynolds numbers of 500, 750, 1000, and 1650. The results of the numerical simulations were similar with those of the experiments; the heat transfer coefficients of the numerical results were smaller than those of the experimental results. The reason for the lower heat transfer coefficients for

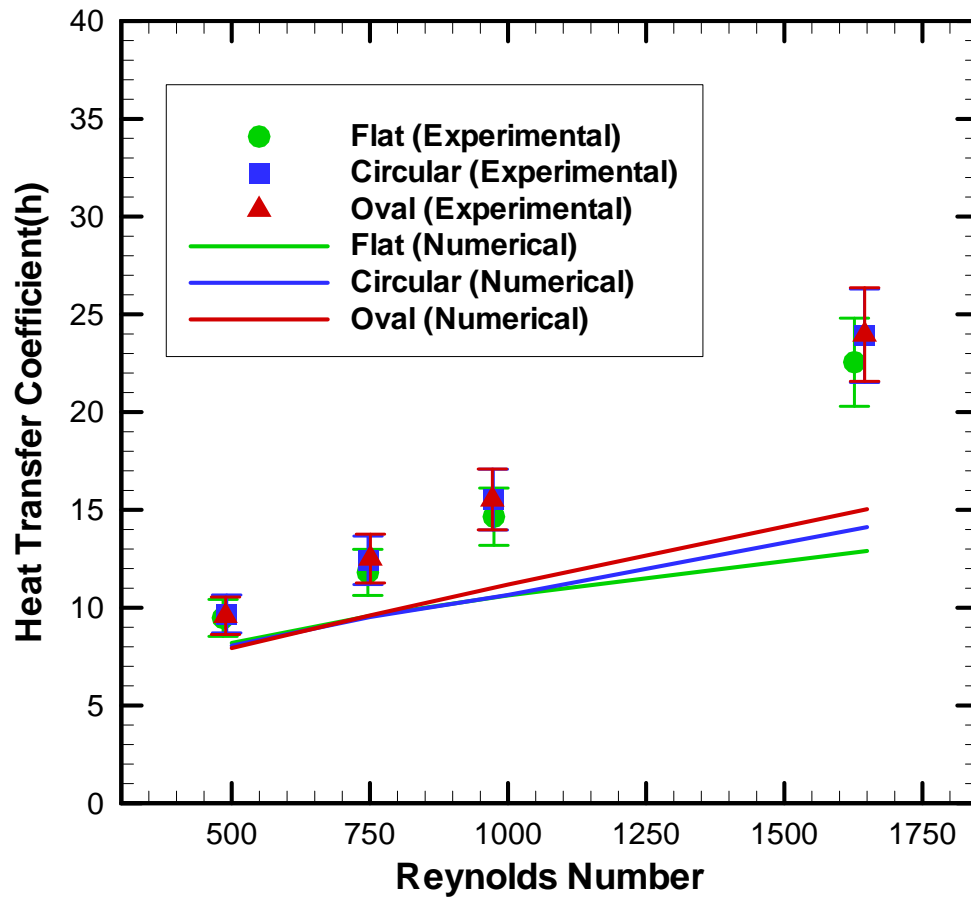


Fig. 5.3 Heat transfer enhancement on the dimple plates

the numerical results is that the boundary condition of the numerical study was different with the boundary condition of the experiment. In case of the numerical study, heat loss to the outside surroundings was not included. If the boundary condition for the numerical study was applied the same as the experiment, the difference between numerical and experimental results should be smaller than the obtained.

5.3.2 Pressure Drop

Fig 5.4 shows the friction factor ratio, f/f_0 for circular and oval type dimpled plates for the four different Reynolds numbers of 500, 750, 1000, and 1650. The pressure drops of the dimpled plates for a laminar airflow are either equivalent to, or less than values produced in the flat plate with no dimples.

In the case of the circular dimpled plate, the friction factor ratio, f/f_0 was roughly 0.94. The friction factor ratio, f/f_0 for the oval dimpled plate was roughly 0.89. The pressure drop for the oval type dimpled plate was smaller than that of the circular type dimpled plate.

5.3.3 Thermal Performance

The thermal performance factor was evaluated with Eq. 5.1 using the average Nusselt number ratio and the friction factor ratio. This parameter compares the heat transfer enhancement by dimples per unit pumping power relative to the heat transfer for the flat plate.

$$TP = (Nu / Nu_0)(f / f_0)^{-1/3} \quad (5.1)$$

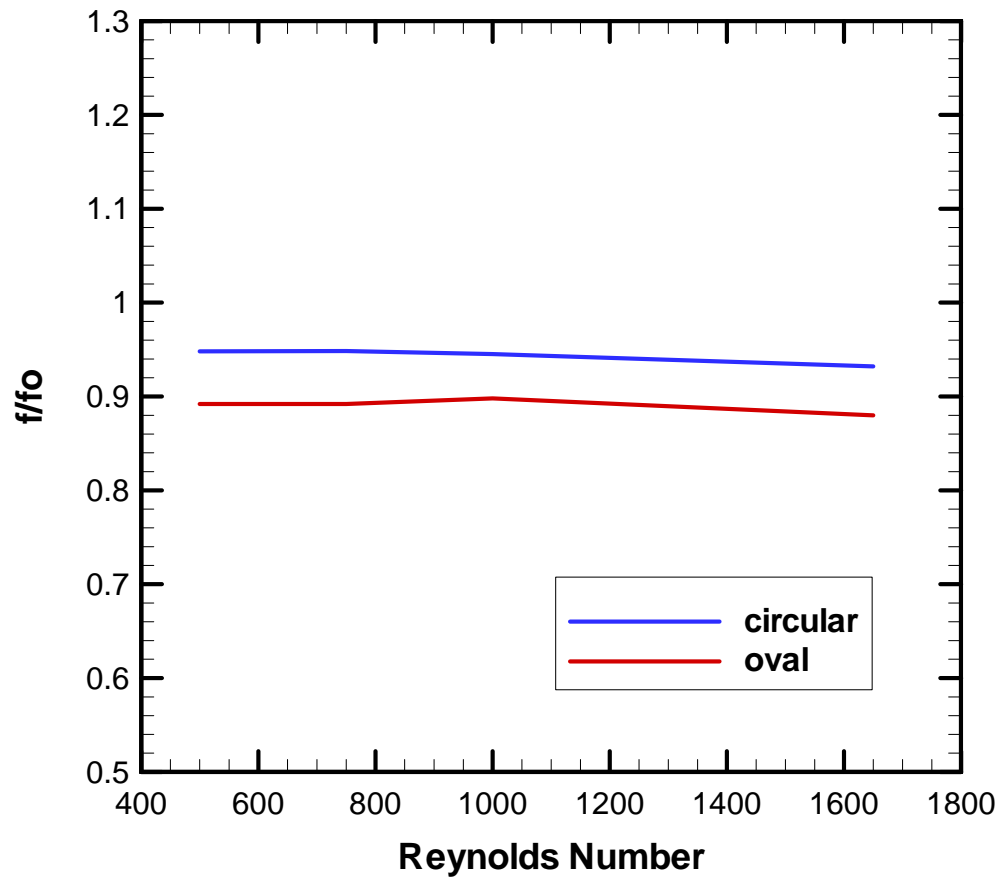


Fig. 5.4 Friction factor ratio, f/f_0

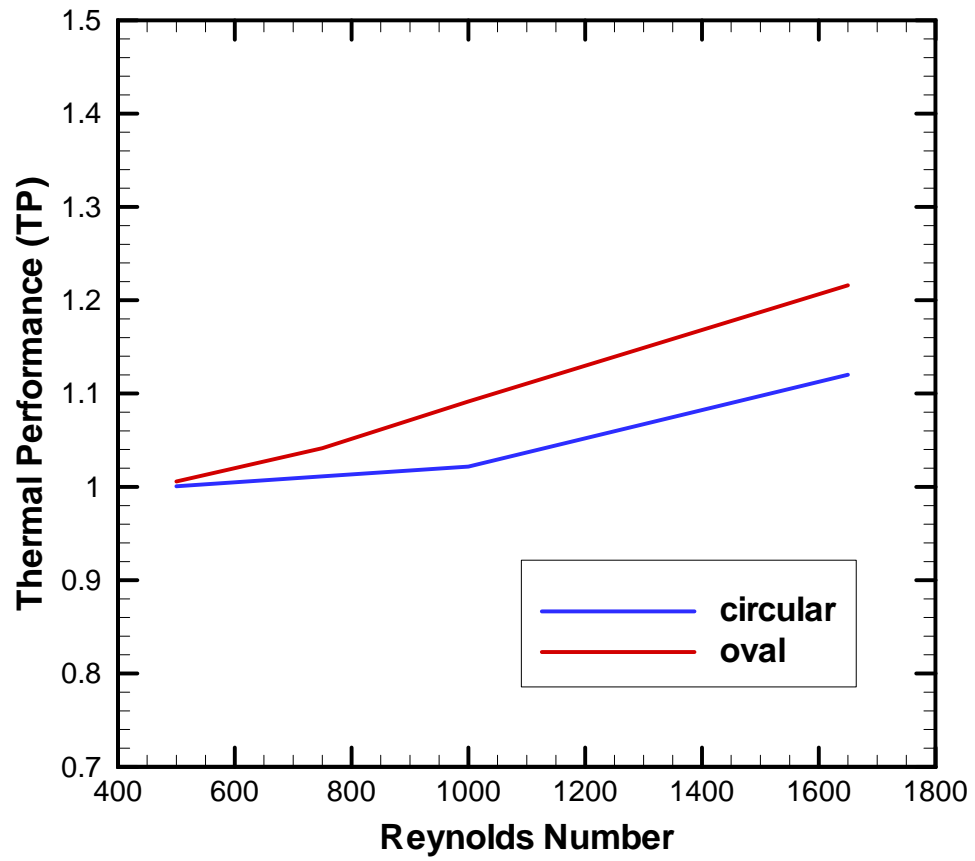


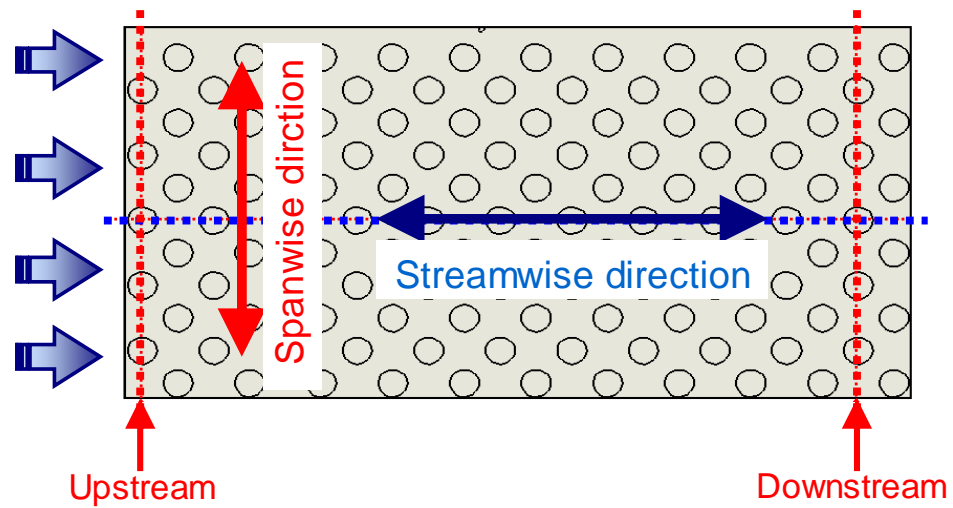
Fig. 5.5 Thermal performance for circular and oval dimpled plate

Fig 5.5 compares the thermal performance factor for two different dimpled plates: circular and oval dimpled plate. Both cases showed that the thermal performance factor increases with increasing mass flow rate. The thermal performance factor for the oval dimpled plate increased from 1.0 to 1.21. The thermal performance factor for the circular dimpled plate increased from 1.0 to 1.12. The factor for the oval type dimpled plate was larger than that of the circular dimpled plate for all cases.

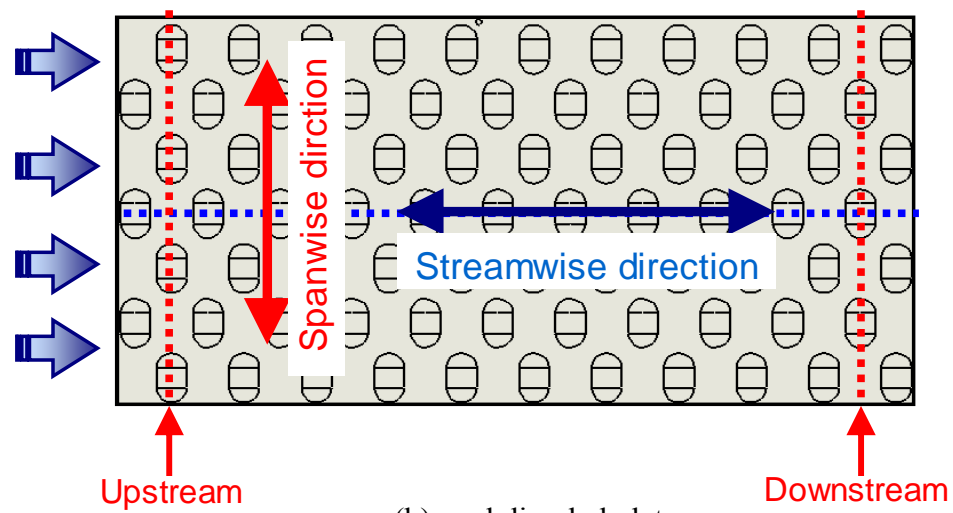
5.3.4 Flow Structure

The flow structure was investigated by analyzing the numerical model. The streamwise sectional view, spanwise sectional view, topview over a dimple, and topview inside of a dimple were plotted which enabled the flow structure to be visualized.

Fig. 5.6 shows the schematic diagram for circular and oval dimpled plates, which were employed. Fig 5.7 shows the streamwise sectional view of the flat plate for Re_H500 and Re_H1650 . In Fig. 5.7, the streamlines are displayed for each case. In the case for Re_H1650 , stronger and larger recirculation regions exist for both the upstream and downstream region. Figs, 5.8 and 5.9 show streamwise section view of the circular and oval dimpled plate for Re_H500 and Re_H1650 respectively. Similar to the flat plate configuration, stronger and larger recirculation regions exist for both the upstream and downstream region at Re_H1650 . The vortexes inside of the dimples are shown at the downstream region for both the circular and oval dimpled plates. Reattachment is evident at the landing area of the dimples at the downstream regions. The flow reattachment enhances the local convection heat transfer. On the other hand, a recirculation zone reduces heat convection because the flow is trapped in that zone.



(a) circular dimpled plate



(b) oval dimpled plate

Fig. 5.6 Schematic diagram of planes used to compute the streamwise development over dimples

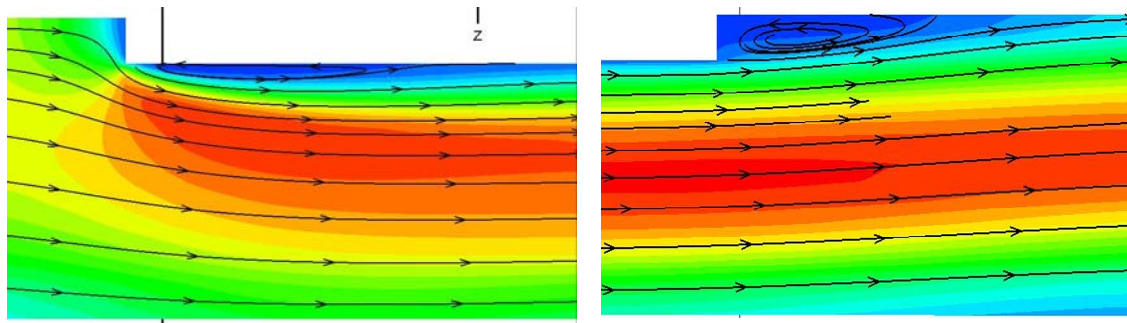
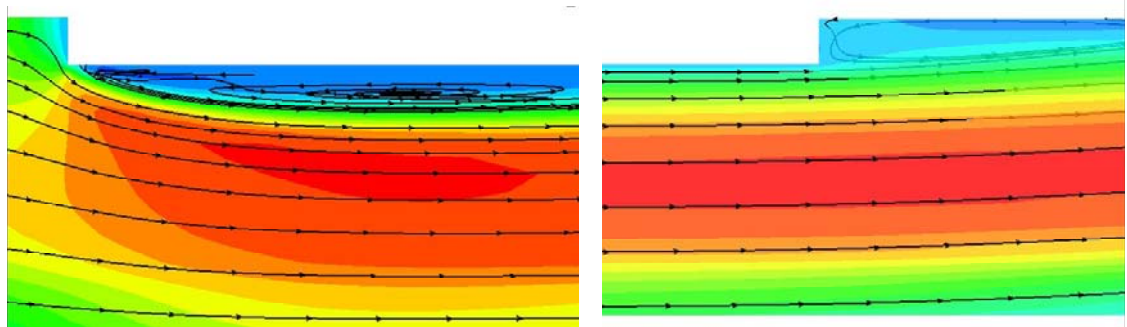
(a) upstream for $Re_H 500$ (b) downstream for $Re_H 500$ (c) upstream for $Re_H 1650$ (d) downstream for $Re_H 1650$

Fig. 5.7 Streamline of upstream and downstream for the flat plate

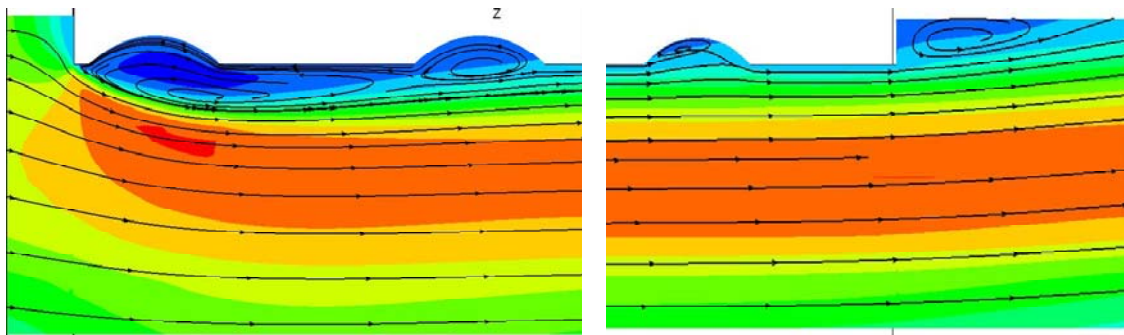
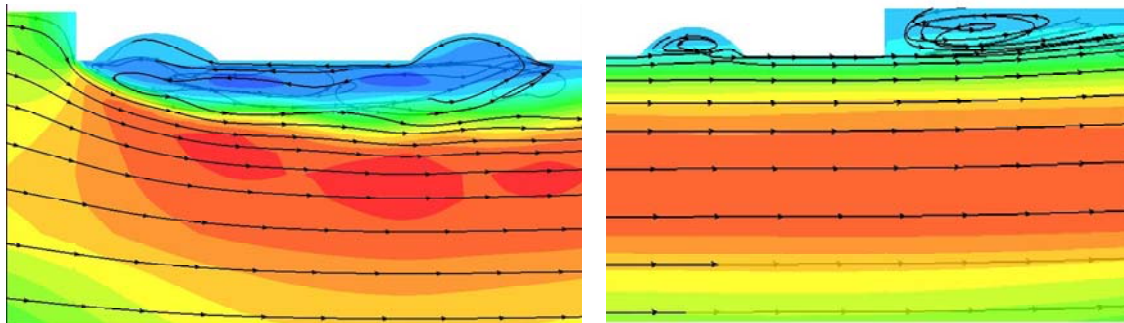
(a) upstream for $Re_H 500$ (b) downstream for $Re_H 500$ (c) upstream for $Re_H 1650$ (d) downstream for $Re_H 1650$

Fig. 5.8 Streamline of upstream and downstream for the circular dimpled plate

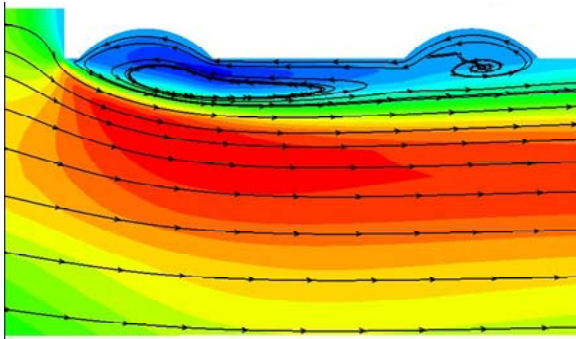
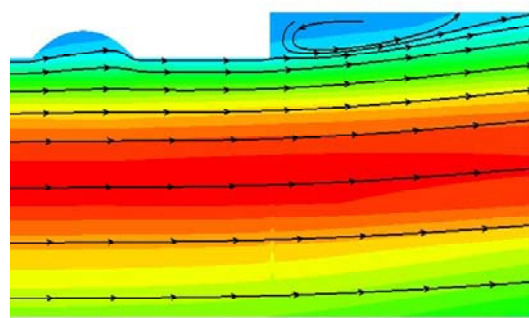
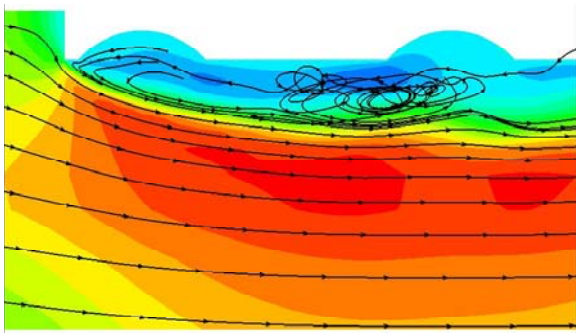
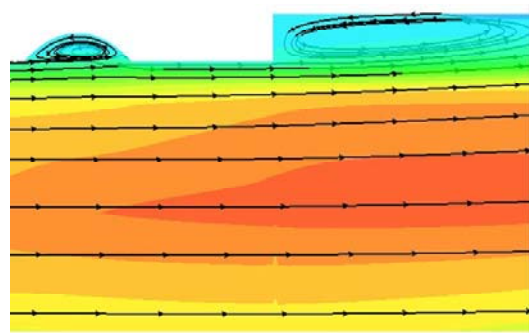
(a) upstream for $Re_H 500$ (b) downstream for $Re_H 500$ (c) upstream for $Re_H 1650$ (d) downstream for $Re_H 1650$

Fig. 5.9 Streamline of upstream and downstream for the oval dimpled plate

Figs, 5.10 and 5.11 show downstream spanwise sectional views of the circular and oval dimple plate, respectively. In Figs, 5.10 and 5.11, the secondary vortices are evident around the spanwise corner of the circular and oval dimples. This secondary vortices also enhance the local convection heat transfer due to the reattachment.

Fig 5.12 shows the top view over the flat plate. In Fig. 5.12, the streamlines are parallel to the airflow direction for both upstream and downstream regions. Fig. 5.13 shows the top view over the circular dimpled plate. At the upstream, streamlines are parallel to the airflow direction for both Re_H500 and Re_H1650 . However, streamlines at the downstream are not parallel to the airflow direction for both Re_H500 and Re_H1650 . In the case of Re_H1650 , streamlines are more deflected in the spanwise direction due to the primary and secondary vortices. Fig. 5.14 shows the streamwise top view over the oval dimpled plate and the trend of the streamline direction is similar to the case for the circular dimpled plate.

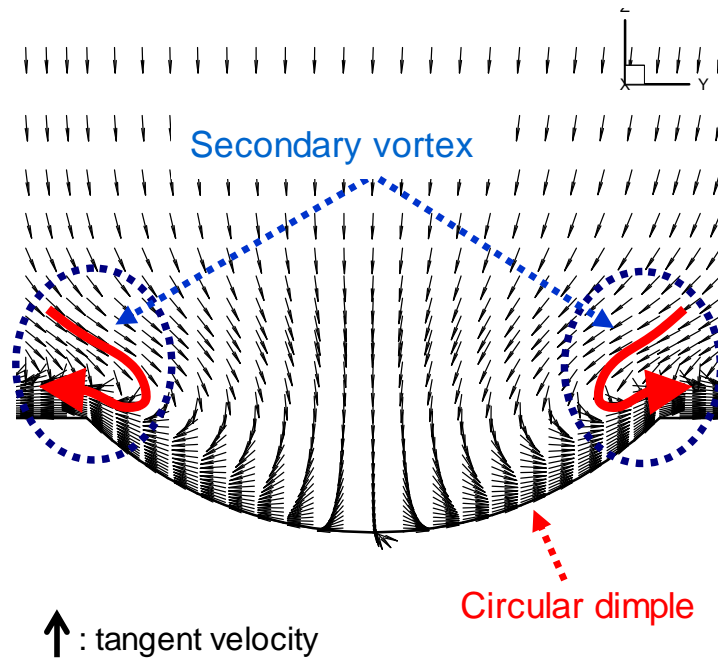
Fig. 5.15 shows the topview inside of the circular and oval dimples for Re_H500 and Re_H1650 at the downstream region. In Fig. 5.15, higher intensity recirculation is shown for Re_H1650 comparing to the case for Re_H500 . In case of the oval dimple, the larger recirculation inside of the dimple enhances the flow mixing leading to increase heat transfer.

5.4 Summary of Experimental Results and Numerical Predictions

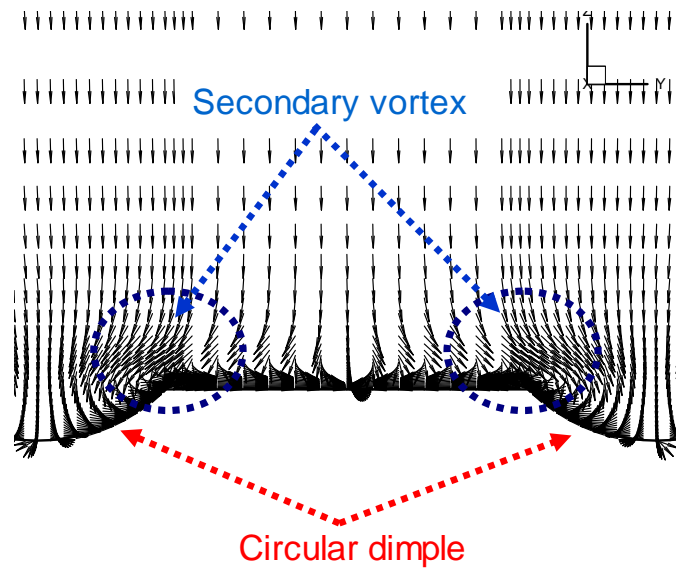
Using an experimental method, the heat transfer coefficient of the three copper plates was calculated. The value was increased with increasing mass flow rate. At very

low flow velocity (Reynolds number based on channel height $Re_H=500$), the ratio for Nu/Nu_0 for circular and oval type dimpled plate is less than 1.02. For Reynolds number from 750 to 1650, Nu/Nu_0 ratios for both circular and oval cases were approximately around 1.11 regardless of Re_H .

Numerical studies for the same geometries and test conditions with the experimental study were conducted. The heat transfer coefficients of the numerical results are similar with those of the experiment results, but the heat transfer coefficients of the numerical results are smaller than those of the experiments. The pressure drops of the dimpled plates for a laminar airflow are either equivalent to, or less than values produced in a flat plate with no dimples. As the airflow velocity gets faster, the thermal performances of circular and oval plates increased. Generally, the thermal performance of the oval type plate was higher than that of the circular dimples. Both the circular and oval dimpled plates show that a primary vortex pair results from the recirculation region inside of the dimples. Primary vortices are positioned in the upstream of the dimple. From each side of dimples, the second vortex flows are observed. The reattachment of the central and secondary vortex flow occurred at the trailing edge.

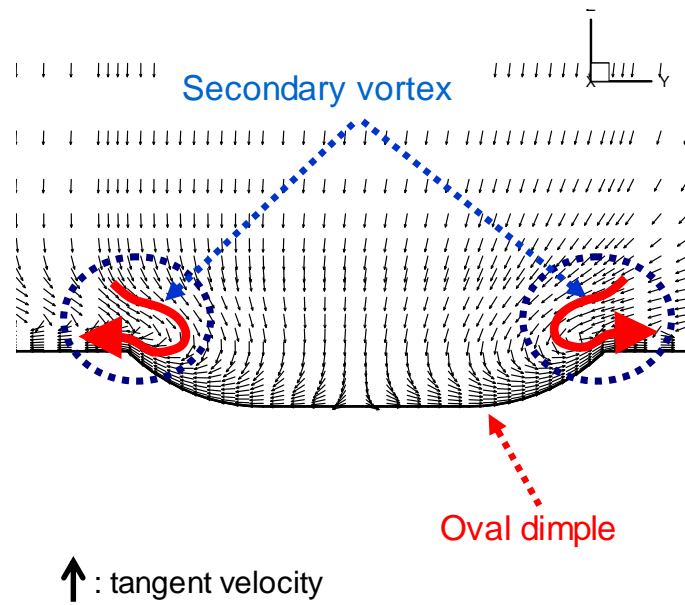


(a) downstream spanwise section for the circular dimpled plate for $Re_H 500$

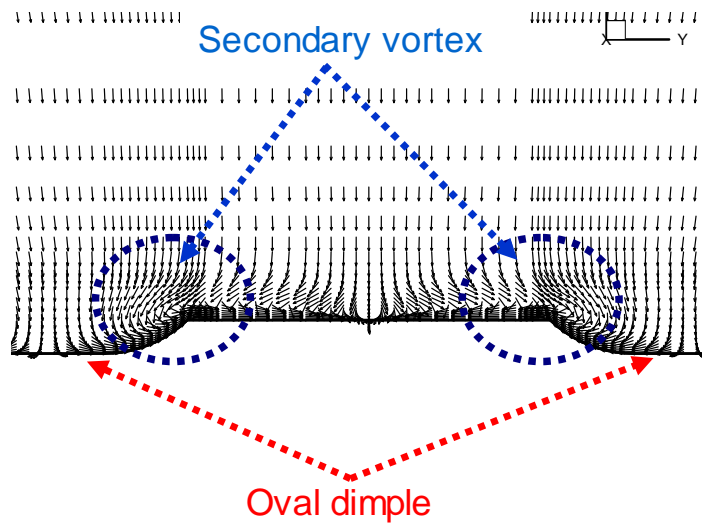


(b) downstream spanwise section for the circular dimpled plate for $Re_H 500$

Fig. 5.10 Downstream spanwise sectional view for the circular dimpled plate

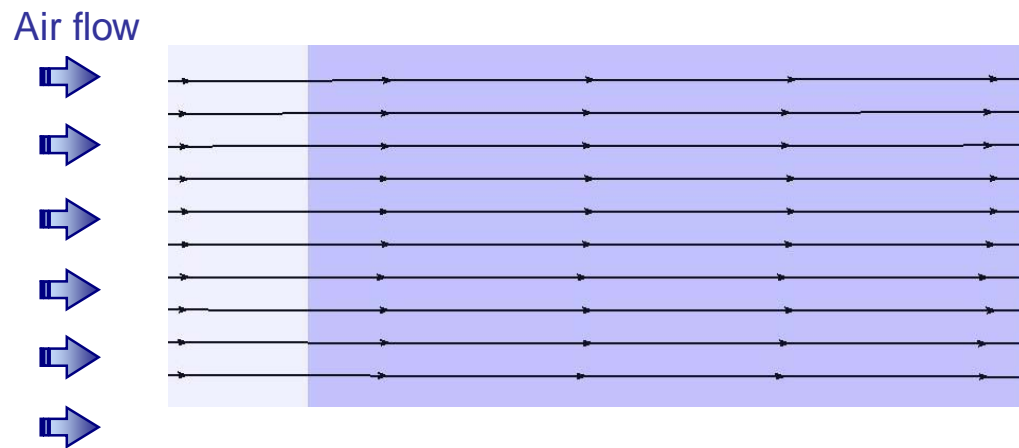


(a) downstream spanwise section for the oval dimpled plate for $Re_H 500$

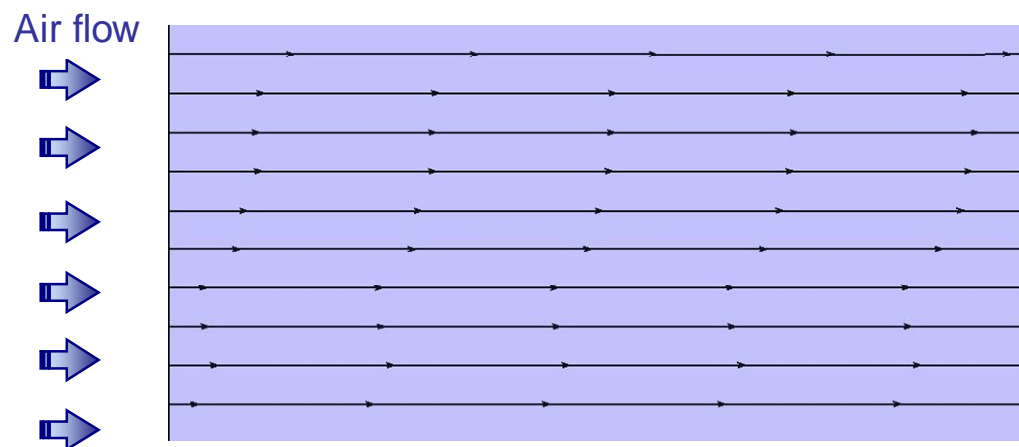


(b) downstream spanwise section for the circular dimpled plate for $Re_H 500$

Fig. 5.11 Downstream spanwise sectional view for the oval dimpled plate



(a) upstream region for the flat plate



(b) downstream region for the flat plate

Fig. 5.12 Streamwise top view over the flat plate

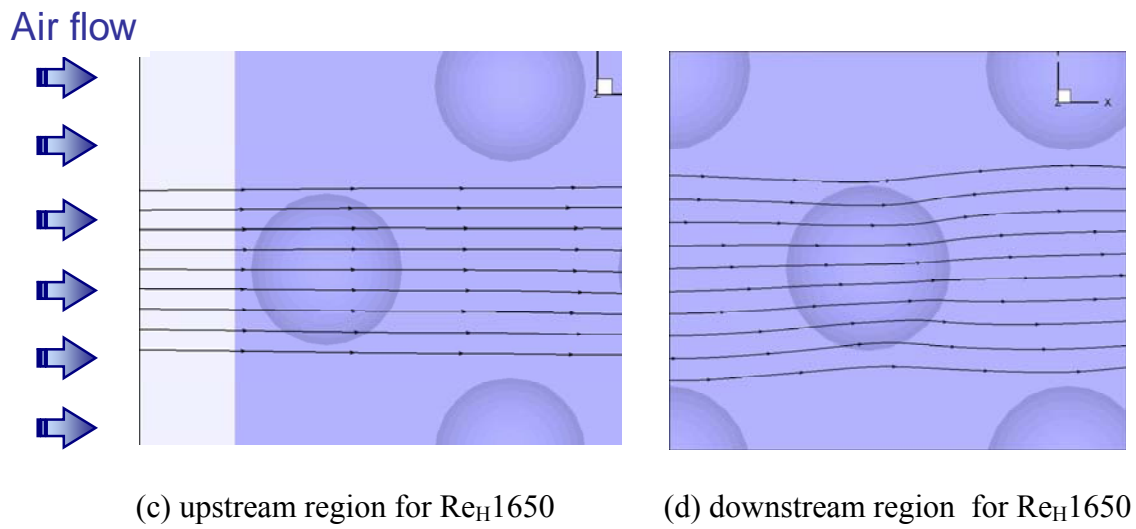
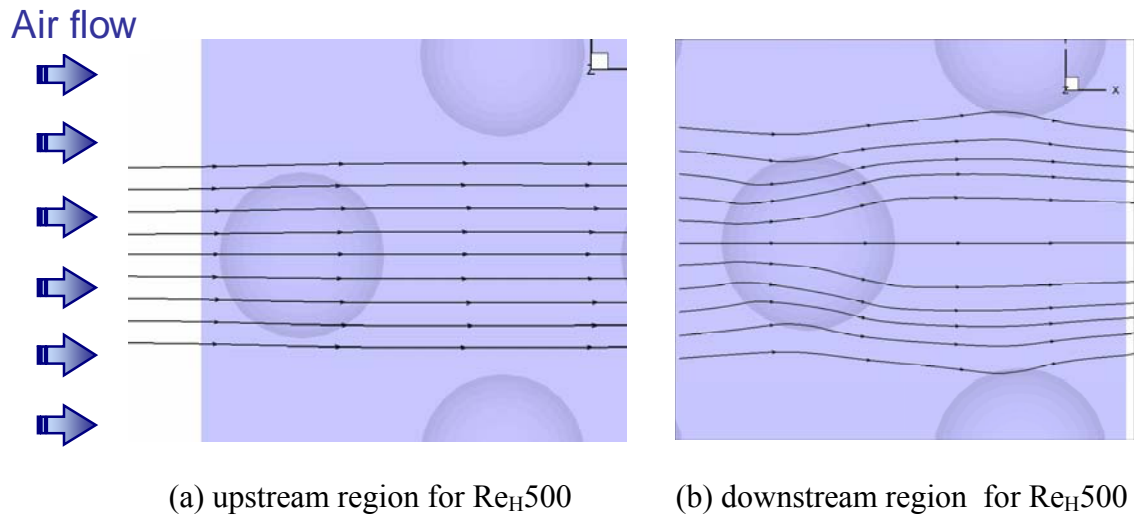


Fig. 5.13 Streamwise top view over the circular dimpled plate

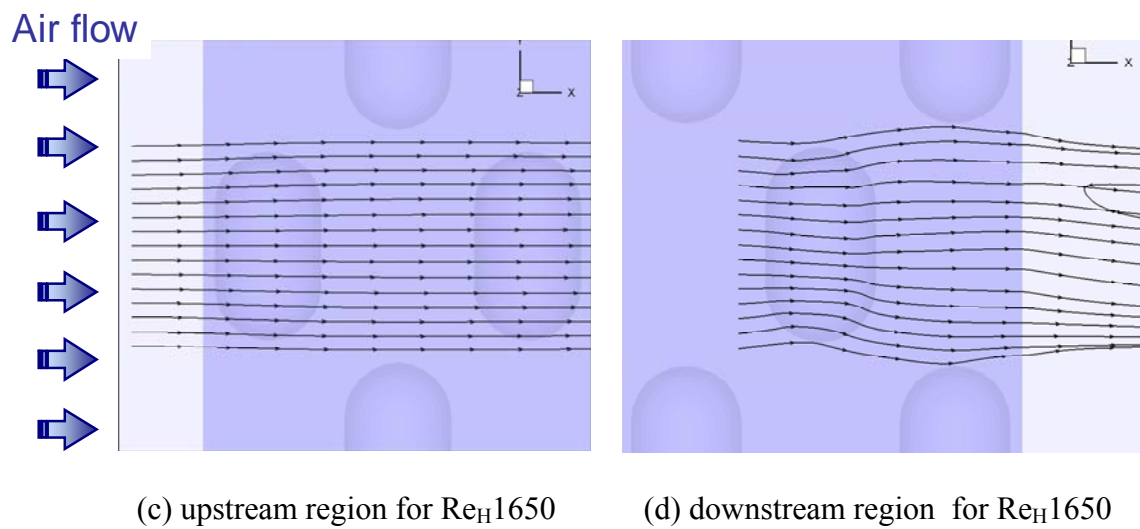
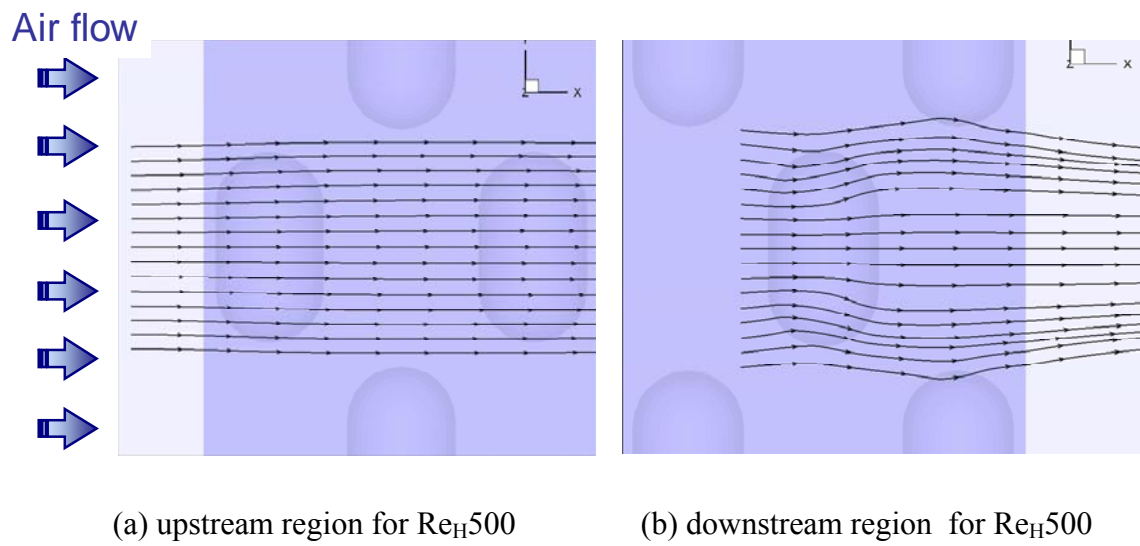


Fig. 5.14 Streamwise top view over the oval dimpled plate

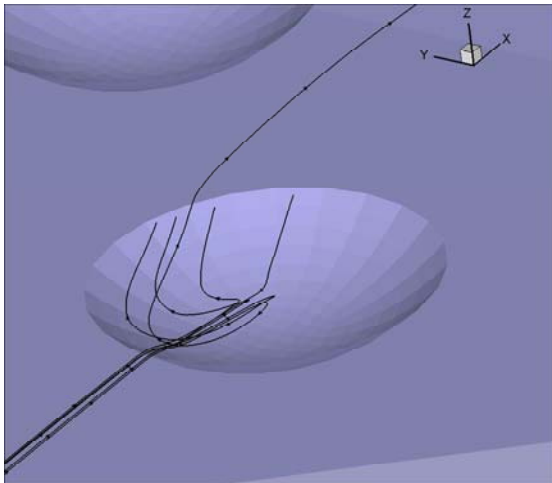
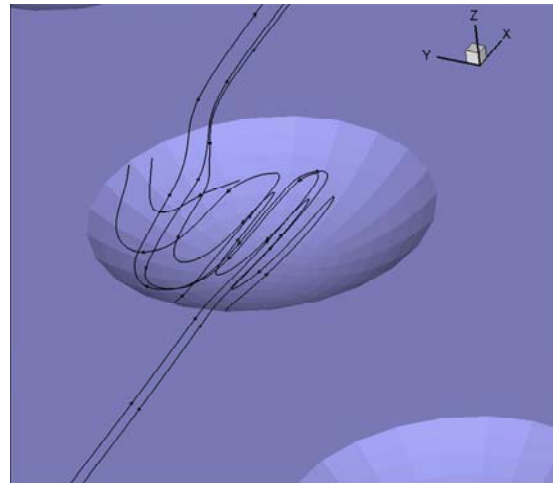
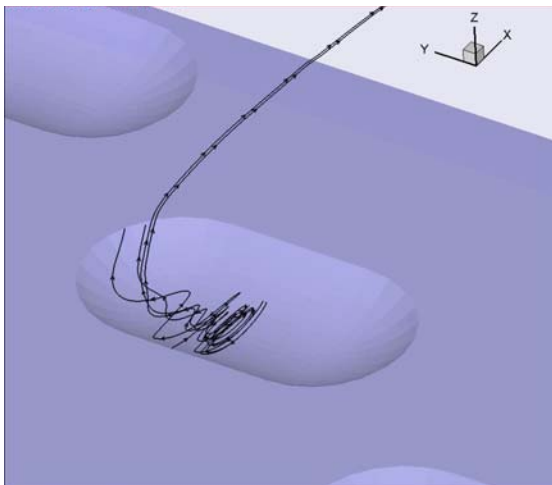
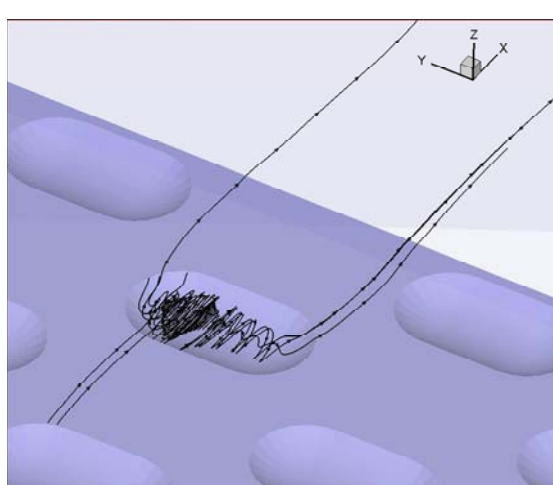
(a) downstream region for $Re_H 500$ (b) downstream region for $Re_H 16500$ (c) downstream region for $Re_H 500$ (d) downstream region for $Re_H 16500$

Fig. 5.15 Streamwise top view inside of the dimples

CHAPTER VI

CONCLUSIONS AND RECOMMENDATIONS

This investigation presents experimental and numerical results for the heat transfer characteristics of a heat sink for laminar airflow conditions using two different types of dimples. The average heat transfer and heat transfer enhancement were obtained experimentally. Heat transfer, pressure drop, thermal performance and flow conditions were numerically simulated.

Experiments using copper plates with a flexible heater were conducted to obtain heat transfer characteristics for a heat sink with dimpled surfaces in laminar airflow. Three different copper plates were fabricated and used to obtain the average heat transfer: flat, circular, and oval dimpled plates. Dimples were placed on both side of the copper plate. Each plate was located in the middle of the rectangular channel and a uniform heat flux was applied from the top of the plate. The flat plate was used for baseline data. The findings of this experimental study are summarized as follows:

1. The heat transfer coefficient of the three copper plates increased with increasing mass flow rate,
2. At very low flow velocity (Reynolds number based on channel height $Re_H=500$), the ratio for Nu/Nu_0 for circular and oval type dimpled plate is less than 1.02,
3. For Reynolds number from 750 to 1500, Nu/Nu_0 ratios for both circular and oval cases were approximately around 1.11 regardless of Re_H .

The same geometries and test conditions with the experimental study were used to simulate heat transfer coefficient, pressure drop, thermal performance, and flow by using FLUENT version 6.2.16. The findings of this numerical study are summarized as follows:

1. The heat transfer coefficients of the numerical results are very similar with those of the experiment results, but the heat transfer coefficients of the numerical results are smaller than those of the experiments,
2. The pressure drops of the dimpled plates for a laminar airflow are either equivalent to, or less than values produced in a flat plate with no dimples. The pressure drop of the oval type dimpled plate is smaller than that of the circular type dimpled plate,
3. As the airflow velocity gets faster, the thermal performances of circular and oval plates increased. Generally, the thermal performance of the oval type plate was higher than that that of the circular dimples,
4. Both the circular and oval dimpled plates show that a prime vortex pair results from the recirculation region inside of the dimples. Primary vortexes are positioned in the upstream of the dimple. As the airflow gets faster, the primary vortexes are also extended in the downstream direction and gets lager in strength. The oval type plate has lager primary vortexes than the circular plate at the same airflow condition.

5. From each side of dimples, the second vortex flows are observed. The reattachment of the central and secondary vortex flow occurred at the trailing edge.

Therefore, from the experimental and numerical studies heat transfer enhancement was observed for all dimpled surfaces. Generally, for turbulators, heat transfer enhancement can be expected, but the pressure penalties can be also expected. On the other hand, dimples enhanced heat transfer from its surface for laminar air flows while the pressure drop was equivalent or smaller than that of the flat surface. These surfaces do indeed enhance thermal performance without the penalty associated with higher pressure drops. Through these observations, we conclude that dimple surfaces have the possibility to be employed in heat sink applications for laminar airflow conditions.

REFERENCES

- [1] P.W. Bearman and J.K. Harvey, Control of circular cylinder flow by the use of dimples, *AIAA J.* 31 (1993) 1753-1756.
- [2] M.K. Chyu, Y. Yu, H. Ding, J.P. Downs and F.O. Soechting, Concavity enhanced heat transfer in an internal cooling passage, *International Gas Turbine & Aeroengine Congress & Exhibition ASME paper 97-GT-437*.
- [3] H.K. Moon, T. O'Connell and B. Glezer, Channel height effect on heat transfer and friction in a dimpled passage, *J. Gas Turbine Power* 122 (2000) 307-313.
- [4] G.I. Mamood, M.L. Hill, D.L. Nelson, P.M. Ligrani, H.K. Moon and B. Glezer, Local heat transfer and flow structure on and above a dimpled surface in a channel, *J. Turbomachinery* 123 (2001) 115-123.
- [5] P.M. Ligrani, G.I. Mamood and M.Z. Sabbagh, Heat transfer in a channel with dimples and protrusion on opposite walls, *J. Thermophys. Heat Transfer* 15 (3) (2001) 275-283.
- [6] G.I. Mahmood and P.M. Ligrani, Heat Transfer in a dimpled channel: combined influences of aspect ratio, temperature ratio, Reynolds number, and flow structure, *Int. J. heat Mass Transfer* 45 (2002) 2011-2020.
- [7] N.K. Burgess and P.M. Ligrani, Effects of dimple depth on channel nusselt numbers and friction factors, *J. Heat Transfer* 127 (8) (2005) 839-847.

- [8] P.M. Ligrani, N.K. Burgess and S.Y. Won, Nusselt numbers and flow structure on and above a shallow dimpled surface within a channel including effects of inlet turbulence intensity level, *J. Turbomachinery* 127 (2005) 321-330.
- [9] R.S. Bunker and K.F. Donellan, Heat transfer and friction factors for flow inside circular tubes with concavity surfaces, *J. Turbomachinery* 125 (4) (2003) 665-672.
- [10] J.C. Han, Turbine blade cooling studies at Texas A&M University: 1980–2004, *J. Thermophys. Heat Transfer* 20 (2) (2006) 161-187.
- [11] S.W. Chang, Y.J. Jan and S.F. Chang, Heat transfer of impinging jet-array over convex-dimpled surface, *Int. J. Heat Mass Transfer* 49 (2006) 3045–3059.
- [12] E. Small, S.M. Sadeghipour and M. Asheghi, Heat Sinks With Enhanced Heat Transfer Capability for Electronic Cooling Applications, *J. Electronic Packaging* 128 (2006) 285-290.
- [13] Y.L. Lin, T. I. Shih and M.K. Chyu, Computations for flow and heat transfer in a channel with rows of hemispherical cavities, *Int. Gas Turbines Aeroengine Congress and Exhibition ASME paper 99-GT-263*.
- [14] S.A Isaev, A.I. Leontiev, A.E. Usachev and D.P. Frolov, Numerical simulation of laminar incompressible three-dimensional flow around a dimple (vortex

dynamics and heat transfer), Russian Ministry of Science and Technology Institute for High-Performance Computing and Databases preprint (1997) 6-67.

- [15] S.A. Isaev, A.I. Leontiev, K.T. Metov and V.B. Kharchenko, Modeling of the influence of viscosity on the tornado heat exchange in turbulent flow around a small hole on the plane, *J. Engineering Physics Thermophys.* 75 (4) (2002) 890 - 898.

- [16] S.A. Isaev, A.I. Leontiev, K.T. Metov and V.B. Kharchenko, Verification of the multiblock computational technology in calculating laminar and turbulent flow around a spherical hole on a channel wall, *J. Eng. Phy. Thermophys.* 75 (5) (2002) 1155-1158.

- [17] S.A. Isaev and A.I. Leontiev, Numerical simulation of vortex enhancement of heat transfer under conditions of turbulent flow past a spherical dimple on the wall of a narrow channel, *High Temperature* 41 (5) (2003) 665-679.

- [18] S.A. Isaev, A.I. Leontiev, P.A. Baranov, K.T. Metov and A.E. Usachev, Numerical analysis of the effect of viscosity on the vortex dynamics in laminar separated flow past a dimple on a plane with allowance for its asymmetry, *J. Eng. Phys. Thermophys.* 74 (2) (2001) 339-346.

- [19] S.A. Isaev, A.I. Leontiev and P.A. Baranov, Identification of self-organized vortex-like structures in numerically simulated turbulent flow of a viscous

incompressible liquid streaming around a well on a plane, *Technical Phys. Letters* 26 (1) (2000) 15-18.

- [20] J. Park, P.R. Desam and P.M. Ligrani, Numerical predictions of flow structures above a dimpled surface in a channel, *Numerical Heat Transfer* 45 (2004) 1-20.
- [21] J. Park and P.M. Ligrani, Numerical predictions of heat transfer and fluid flow characteristics for seven different dimpled surfaces in a channel, *Numerical Heat Transfer* 47 (2005) 209–232.
- [22] K.Y. Kim and J.Y. Choi, Shape optimization of a dimpled channel to enhance turbulent heat transfer, *Numerical Heat Transfer* 48 (2005) 901–915.
- [23] C. Silva, E. Marotta and L. Fletcher, Flow structure and enhanced heat transfer in channel flow with dimpled surfaces: application to heat sinks in microelectronic cooling, *J. Electronic Packaging* 5 (2007) 1129.
- [24] H.W. Coleman and W.G. Steele, *Experimental and uncertainty analysis for engineers*, John Wiley & Son, New York, NY, 1989

APPENDIX A
ERROR ANALYSIS

Uncertainty Analysis

Based on a confidence level of 95% described by Kline and McClintock [24], uncertainty value of $\pm 0.5\%$ for all properties of the air, and $\pm 0.5\%$ for all physical dimensions were used.

To quantify the air mass flow rate, the following expression was used:

$$\dot{m} = \frac{\pi}{4} d_o^2 C Y \left[\frac{2 p_o \Delta p_o}{R T_o (1 - \eta^4)} \right]^{1/2} \quad (\text{A.1})$$

where \dot{m} is the air mass flow rate, d_o is the diameter of the orifice, C is the discharge coefficient, Y is the expansion coefficient, p_o is the pressure at the tap upstream of the orifice, Δp_o is the pressure drop across the orifice, R is the universal gas constant for air, T_o is the temperature at the orifice, and η is the orifice-diameter-to-pipe-diameter ratio.

The uncertainty of an air mass flow rate was determined by Eq. A.2:

$$\frac{\omega_{\dot{m}}}{\dot{m}} = \left[\left(\frac{2\omega_{d_o}}{d_o} \right)^2 + \left(\frac{\omega_C}{C} \right)^2 + \left(\frac{\omega_Y}{Y} \right)^2 + \left(\frac{1}{2} \frac{\omega_{p_o}}{p_o} \right)^2 + \left(\frac{1}{2} \frac{\omega_{\Delta p_o}}{\Delta p_o} \right)^2 + \left(-\frac{1}{2} \frac{\omega_R}{R} \right)^2 + \left(-\frac{1}{2} \frac{\omega_{T_o}}{T_o} \right)^2 + \left(-\frac{1}{2} \frac{\omega_{\eta}}{\eta} \right)^2 \right]^{1/2} \quad (\text{A.2})$$

Based on the maximum uncertainties of measured data in Table A.1, the maximum uncertainty of the air mass flow rate was calculated to be $\pm 2.8\%$.

To quantify the Reynolds number, the following expression was used:

$$\text{Re}_H = \frac{4\dot{m}}{\pi d_p \mu} \quad (\text{A.3})$$

where d_p is the diameter of the pipe at the orifice and μ is dynamic viscosity of air.

The uncertainty of the Reynolds number was determined by Eq. A.4:

$$\frac{\varpi_{\text{Re}}}{\text{Re}_H} = \left[\left(\frac{\varpi_{\dot{m}}}{\dot{m}} \right)^2 + \left(-\frac{\varpi_{\mu}}{\mu} \right)^2 + \left(-\frac{\varpi_{d_p}}{d_p} \right)^2 \right]^{1/2} \quad (\text{A.4})$$

Based on the maximum uncertainties for the air mass flow rate, the dynamic viscosity of air, and the diameter of the pipe, the maximum uncertainty of the Reynolds number is $\pm 2.9\%$.

The uncertainty of the Nusselt number was determined by Eq. A.5

$$\frac{\varpi_h}{h} = \left[\left(\frac{\varpi_{Q_{\text{total}}}}{Q_{\text{total}} - Q_{\text{loss}}} \right)^2 + \left(\frac{\varpi_{Q_{\text{loss}}}}{Q_{\text{total}} - Q_{\text{loss}}} \right)^2 + \left(-\frac{\varpi_{A_s}}{A_s} \right)^2 + \left(-\frac{\varpi_{T_w}}{T_w - T_b} \right)^2 + \left(-\frac{\varpi_{T_b}}{T_w - T_b} \right)^2 \right]^{1/2} \quad (\text{A.5})$$

Based on the maximum uncertainties of measured data in Table A.2, the maximum uncertainty of the heat transfer coefficient was calculated to be $\pm 7.8\%$.

Maximum uncertainties of all calculated data were shown in Table A.3

Table A.1 Maximum uncertainties of measured data for air mass flow rate

Parameter	$\frac{\varpi_{d_o}}{d_o}$	$\frac{\varpi_{C_o}}{C_o}$	$\frac{\varpi_{Y}}{Y_o}$	$\frac{\varpi_{p_o}}{p_o}$
Uncertainty	$\pm 0.5\%$	$\pm 1.0\%$	$\pm 1.0\%$	$\pm 1.0\%$
Parameter	$\frac{\varpi_{\Delta p_o}}{\Delta p_o}$	$\frac{\varpi_R}{R_o}$	$\frac{\varpi_{T_o}}{T_o}$	$\frac{\varpi_{\eta}}{\eta}$
Uncertainty	$\pm 4.1\%$	$\pm 0.5\%$	$\pm 3.0\%$	$\pm 0.5\%$

Table A.2 Maximum uncertainties of measured data for heat transfer coefficient

Parameter	$\frac{\varpi_{Q_{total}}}{Q_{total} - Q_{loss}}$	$\frac{\varpi_{Q_{loss}}}{Q_{total} - Q_{loss}}$	$\frac{\varpi_{A_S}}{A_S}$	$\frac{\varpi_{T_w}}{T_w - T_b}$	$\frac{\varpi_{T_b}}{T_w - T_b}$
Uncertainty	±3.1%	±5.4%	±0.5%	±3.0%	±3.5%

Table A.3 Maximum uncertainties of all calculated data

Parameter	Uncertainty
Mass flow rate, \dot{m}	±2.8%
Reynolds number, Re	±2.9%
Average heat transfer coefficient, h	±7.8%

VITA

Name: Do Seo Park

Address: Department of Mechanical Engineering
Texas A&M University
College Station, Texas 77843-3123

Email Address: pdoseo@tamu.edu

Education: B.En., Mechanical Engineering, Korea University, Korea, 2002
M.S., Mechanical Engineering, Texas A&M University, 2007